QUATIFYING PROCESS-BASED CONTROLS ON COMPENSATIONAL

STACKING OF CHANNELIZED SEDIMENTARY DEPOSITS

A THESIS

SUBMITTED ON THE FOURTEENTH OF DECEMBER 2011

TO THE DEPARTMENT OF EARTH AND ENVIRONMENTAL SCIENCES

IN PARTIAL FULFILLMENT OF THE REQUIREMENTS

OF THE SCHOOL OF SCIENCE AND ENGINEERING

OF TULANE UNIVERSITY

FOR THE DEGREE

OF

MASTER OF SCIENCE

BY

____

Yinan Wang

APPROVED:__________________________

Kyle M. Straub, Ph.D.
Director

____

Nancye H. Dawers, Ph.D.

____

Nicole M. Gasparini, Ph.D

ACKNOWLEDGEMENT

In the Asian cultures, there are two kinds of apprentices with special significance. One is the first apprentice working under the supervision of the master, and the other is the last apprentice accepted by the master right before his/her retirement. Consequently, at the very beginning when I came to Tulane and joined Dr. Straub's group as his first student, I felt thrilled and proud, and probably chuckled to myself involuntarily. Looking back now, I feel so lucky to have met Dr. Straub and have the opportunity to work with him. During these two years, I have received excellent research guidance from my advisor. His scientific insights and enduring enthusiasm for research always surprised and inspired me. Without his help and education in the department, it is very likely that I still have not figured out what the spirit of research is. From the bottom of my heart, I appreciate my advisor's effort and patience on me.

Tulane's EES Department is a wonderful studying place for international students. Living in such a different culture made me weak and vulnerable to mistakes and misunderstandings, but people here are friendly, supportive and thoughtful all the time. Particularly I am grateful for the consideration and scholarly advising from Dr. Nicole Gasparini and Dr. Nancye Dawers. They have been true caring educators for me. I also would like to seize this opportunity to thank our lab technician Jennifer Kuykendall for her kind help in the progression of delta experiments.

FORWARD

This thesis is composed into eight main sections: introduction, background, numerical motivation, experimental methods, experimental results, discussion, future research direction and conclusion. Subsections are presented for the experimental results and discussion. A list of figures, tables and simulation codes precedes the main text. Full captions can be found following these items if applicable.

TABLE OF CONTENTS

LIST OF TABLES

LIST OF FIGURES

Chapter 1: INTRODUCTION

Alluvial basins contain the most complete record of information necessary to quantitatively reconstruct paleolandscape dynamics across many time scales (Sloss, 1962; Ager, 1973; Paola, 2000). Unfortunately, we lack a Rosetta Stone for reading this record, and unlocking the wealth of information preserved in stratigraphy has proven difficult. Alluvial deposits also house important groundwater and hydrocarbon reserves and provide reservoirs in which atmospheric carbon dioxide may be sequestered. Managing these resources in the face of increasing societal demand requires accurate means of predicting and modeling subsurface architecture and sediment patterns based on limited data from wells and reflection seismology.

Sedimentary bodies that arise from depositional processes along passive continental margins also serve as home to millions of people. However, these passive continental margin environments are particularly susceptible to environmental change, resulting from both anthropogenic and natural drivers (Syvitsky et al., 2009), making our ability to unlock paleo-environmental records particularly relevant to our understanding of these systems and our ability to predict future system evolution. As a result, ancient sedimentary context could play an important role in the development of coastal restoration efforts in these environments. For example, a wealth of stratigraphic data exists for the Mississippi River delta region that could be used to define sedimentation rates and surface dynamics during ancient (and potentially future) distributary channel configurations (Stanley et al., 1996; Galloway et al., 2000; Kulp et al., 2002). This type of data, if properly understood, would aid in the planning of delta restoration projects critical for the region's long-term sustainability. Presently, stratigraphic interpretation and prediction is accomplished with largely interpretive, qualitative or semi-quantitative models, severely restricting our ability to extract meaningful quantitative data from the stratigraphic record.

The development of quantitative stratigraphic models began in 1978 with a study by Pitman that presented the first formal analysis of the relation of shoreline to sea-level in the light of tectonic subsidence. Following Pitman (1978), the development of most stratigraphic models has focused on the influence of a system's boundary conditions to resulting stratigraphic architecture (Kendall et al., 1991; Hardy et al., 1998; Csato and Kendall, 2002; Euzen et al., 2004). These boundary conditions include global sea level, tectonic setting, and climate. Unfortunately, developing quantitative stratigraphic models is complicated because the internal dynamics of depositional systems convolve with the external boundary conditions that control basin sedimentation. This internal (or autogenic) variability is often presumed to impart relatively small amplitude, high-frequency noise in sedimentary successions that otherwise reflect large scale external (or allogenic) forcings (Slingerland, 1990). Recent theoretical and experimental work shows that autogenic dynamics in sedimentary systems can occur over large temporal and spatial scales (Sheets et al., 2002; Jerolmack and Paola, 2007; Straub et al., 2009; Ganti et al., 2011). Particularly vexing, these behaviors can produce stratigraphic patterns that are similar to stratigraphic architecture heretofore considered the result of changing climate, tectonics, or sea level (Kim and Paola, 2007; Hajek et al., 2010) and in some cases can destroy or overprint the stratigraphic record of environmental signals (Jerolmack and Paola, 2010).

The terms *allogenic* and *autogenic* grew out of a study by Beerbower (1964) who described cyclic sedimentation patterns as resulting from either internal forcings (*autocyclicity*) or external forcings (*allocyclicity*). Miall (1996) noted that not all internal and external processes are cyclic and introduced the terms autogenic and allogenic. In the last fifteen years, the two terms have been further defined. *Autogenic process* is now used to refer to surface processes and stratigraphic products resulting under steady external dynamic forcings (Blum and Tornqvist, 2000; Swenson et al., 2005; Muto et al., 2007), while *allogenic process* is used to refer to surface processes and stratigraphic products resulting from nonsteady external dynamic forcings (Muto and Swenson 2005; Muto et al., 2007).

Three commonly discussed autogenic processes are lateral river migration, avulsion, and delta-lobe switching (Beerbower, 1965; Coleman, 1988; Miall, 1996; Deptuck et al., 2007). These processes, whether stochastic or cyclic in nature, occur even under constant or steadily changing boundary conditions (Kleinhans, 2005; Muto et al., 2007; Clarke et al., 2010). These processes acting over long time scales determine the evenness or unsteadiness with which basins fill and are controlled by inherent characteristics of sedimentary systems, including channel mobility and the scale of depositional systems with respect to basin size. Consequently, these properties of sediment transport systems can impose first-order controls on fluvial stratigraphy (Muto, 2001; Kim and Paola, 2007; Martin et al., 2009b; Tomer, 2011). However, at present the time scale at which autogenic processes supplant allogenic forcing in different systems is currently unconstrained (Paola et al., 1992; Sheets et al., 2002; Covault et al., 2010). Since the characteristics and relative importance of autogenic processes are still poorly known and difficult to infer from natural sedimentary systems, laboratory experiments have been performed to examine the relationship between autogenic surface dynamics and resulting stratigraphy (Muto and Steel, 2004; Kim and Jerolmack, 2008; Martin et al., 2009b).

The primary objective of the present study is to quantify the tendency of sediment transport systems to evenly fill sedimentary basins through autogenic processes. Secondarily, we aim to determine the time scales necessary for sedimentary deposits to develop shapes set by the basins they are filling. This objective is addressed utilizing physical experiments in a laboratory setting where we monitor the evolution of deltaic systems experiencing constant external forcings, thus isolating autogenic processes and their stratigraphic product.

Chapter 2: BACKGROUND

The majority of work highlighting the presence and importance of autogenic processes has occurred over the last decade and utilized physical laboratory experiments and numerical models (Van Heijst and Postma, 2001; Kubo et al., 2005; Sheets et al., 2007; Hoyal and Sheets, 2009). Experiments like those performed in the Experimental EarthScape (XES) Facility, at St. Anthony Falls Laboratory at the University of Minnesota, allow the sedimentology community to test the response of systems to external forcing under controlled conditions (Heller et al., 2001; Sheets et al., 2002; Kim et al., 2006; Martin et al., 2009b). In many of these experiments autogenic processes were shown to strongly influence the surface dynamics and resulting stratigraphic architecture, even in systems exposed to strong external forcings (Kim et al., 2006; Strong and Paola, 2008; Jerolmack and Paola, 2010).

Results of these physical and numerical modeling studies indicate that the evenness with which a sedimentary system can fill a basin is a first-order control on the degree of organization detected in the surface and stratigraphic evolution of sedimentary systems. Under constant, or even changing boundary conditions, some sedimentary systems tend to move across and fill basins randomly and chaotically, while others deposit in a structured, even manner. For example, highly mobile fan-delta systems modeled in Sheets et al. (2007) can migrate across a basin to fill it much more evenly than more cohesive, laterally-restricted deltaic systems (Hoyal and Sheets, 2009; Edmonds and Slingerland, 2010). Likewise, sedimentary systems that are very large with respect to the size of a basin may be capable of filling space more evenly than smaller systems.

One way of describing how evenly basins fill is by characterizing the degree of compensation observed in a basin fill. Compensation describes the tendency of deposits to preferentially fill topographic lows, smoothing out topographic relief and "compensating" for localized deposition from discrete depositional elements. This tendency is thought to result from periodic reorganization of the sediment transport field to minimize potential energy associated with elevation gradients (Mutti and Sonnino, 1981; Deptuck et al., 2008). Compensational stacking has been used to describe large-scale architecture in deepwater, fluvial, and, deltaic packages (Mohrig et al., 2000; Olariu and Bhattacharya, 2006; Hofmann et al., 2011), wherein avulsions reorganize the sediment transport field along local topographic lows.

Autogenic processes, including characteristic channel avulsion skip-length or frequency, can mediate compensational basin filling. Jerolmack and Paola (2007) show that over long time scales, channel avulsion skip lengths (the cross-stream distance between the abandoned and new channel locations) may be power-law or bimodally distributed leading to a nonrandom (nonuniform or non-Gaussian) stratigraphic organization of alluvial deposits. This process has been shown to result in anti-compensation, as defined by Straub et al. (2009) and produce stratigraphically-clustered channel deposits (Hajek, 2010).

Recently, a metric was developed to quantify the strength of compensation in sedimentary basins by comparing observed stacking patterns to what would be expected from simple, uncorrelated stacking (Straub et al., 2009). Straub et al. (2009) quantified compensation in basin filling by comparing the spatial variability in sedimentation between select depositional horizons with increasing vertical stratigraphic averaging distance:

$$\sigma_{ss}(T) = \left(\int_L \left[\frac{r(T;x)}{\hat{r}(x)} - 1 \right]^2 dL \right)^{1/2} \quad (1)$$

where $r(T;x)$ is the local sedimentation rate measured over a stratigraphic interval T, x is a horizontal coordinate, L is the cross-basin length, and $\hat{r}(x)$ is the local long-term sedimentation (or subsidence) rate. Straub et al. (2009) showed that σ_{ss} decreases with increasing T, following a power law trend in 6 study basins:

$$\sigma_{ss} = aT^{-\kappa} \quad (2)$$

where the exponent, κ, was termed the compensation index and a is a leading coefficient. κ was found theoretically to be 0.5 for random stacking that is uncorrelated in space and time, and 1.0 for perfect compensational stacking. Values less than 0.5 indicate anti-compensation (Figure 1). The decay of σ_{ss} with stratigraphic scale can be understood as follows: over sufficiently long time intervals a transport system is able to visit every spot in a basin repeatedly; consequently the ratio of the sedimentation to subsidence at any point in the basin should approach unity (Figure 1). Over short time intervals, however, depositional geometries within a basin are controlled by the configuration of the transport system. As a result, the ratio of sedimentation to subsidence at any point in the basin is highly variable. Generally as the time scale of averaging increases, this variability diminishes.

The six basins analyzed by Straub et al. (2009) included a range of system scales (experimental basins as well as field scale basins) and a range of depositional environments (fluvial and deep marine stratigraphy). Data describing the decay in the standard deviation of sedimentation/subsidence from the six studied basins was found to scale with the mean channel depth of each system. Channel depth thus emerged as a fundamental length scale in stratigraphic architecture across environments. This approach allows identification of specific time and space scales relevant to stratigraphic architecture. These specific time and space scales, though, were not addressed or identified in the study by Straub et al. (2009). Rather the compensation index characterizing the decay of σ_{ss} was assumed to by constant over all time scales of evolution for each basin studied.

In this study we utilize the compensation index in conjunction with numerical, experimental, and field data to (1) determine how compensation varies with scale, (2) define a compensation time scale that predicts when the transition from autogenic to allogenic deposits is complete, (3) determine if questions (1) and (2) are influenced by the scale of a sediment transport system relative to the size of the basin it is filling, and (4) determine how stratigraphic organization changes from sediment source to sink.

Chapter 3: NUMERICAL MOTIVATION

One autogenic mechanism that results in periodic reconfiguration of transport systems towards topographic lows, and thus might influence the strength of compensation at specific time scales, is avulsion (Mohrig et al., 2000). We explore how avulsions influence compensation using two-dimensional (2D) object-based stacking models. We model basin filling with discrete triangular elements that are meant to represent channel or lobe deposits. During each time step one element is deposited in the basin while the subsidence is set to balance mean basin aggradation. An approximation of the avulsion process is modeled by placing channel elements with the following rules. At every n^{th} time step during basin filling the active channel relocates to the absolute topographic low in the model domain. For all other time steps deposition follows a random walk with elements moving one channel width left or right of the previous element. Figure 2 shows a sample stratigraphic section generated by this model and the corresponding plots of σ_{ss} for three model runs with different avulsion time sales. It can be seen that σ_{ss} decays as a function of T under different avulsion time scales. On these plots, we identify two regimes in the plots of σ_{ss} vs. T where 1) κ increases from a value less than 1.0 to 1.0 and 2) κ equals 1.0.

The time scale at which κ first reaches unity represents a shift from stratigraphy that partially records stochastic autogenic processes to stratigraphy determined purely by regional sediment supply and accommodation. We hypothesize that this transition occurs at the time necessary to generate a deposit with a mean thickness equal to the maximum topographic relief on the transport system at any time (Figure 3). We therefore define a compensation time scale (T_C) as:

$$T_C = \frac{l}{\bar{r}} \qquad (3)$$

where l is a roughness length scale and $\bar{r}$ is the basin wide long-term sedimentation (or subsidence) rate. In our numerical models l represents the maximum amount of topographic mounding that occurs between the avulsions which occur at every n^{th} time step and Eq. 3 correctly predicts the hand-off from stochastic to deterministic dynamics.

Chapter 4: EXPERIMENTAL METHODS

In order to examine 1) the influence of time scale of measurement and 2) ratio of transport system size to basin size on the strength of compensation and organization in stratigraphy, we performed two laboratory experiments (Figure 4). In the last decade a wide variety of studies have investigated the surface dynamics and stratigraphy associated with channelized deltas and deep-water fans at reduced scale (Heller et al., 2001; Van Heijst and Postma, 2001; Metivier et al., 2005; Yu et al., 2006; Hoyal and Sheets, 2009; Martin et al., 2009b). As outlined in a recent review by Paola et al. (2009), these experiments produce spatial structure and kinematics that, although imperfect, compare well with natural systems despite differences of spatial scale, time scale, material properties, and number of active processes. As a result, these experiments have been shown to provide morphodynamic and stratigraphic insight into the evolution of channelized settings under an array of external and internal influence (Whipple et al., 1998; Strong and Paola, 2008; Martin et al., 2009b; Paola et al., 2009). While many challenges exist in directly up-scaling experimental results, several recent studies have demonstrated that utilization of appropriate statistical tools can allow laboratory and field stratigraphy to be compared (Straub et al., 2009; Hajek et al., 2010; Wang et al., 2011).

In many of these experiments detailed topographic measurements were made of the evolving surface in order to characterize topographic attributes (Metivier et al., 2005; Hoyal and Sheets, 2009; Martin et al., 2009b). However, with the exception of a weakly cohesive channelized experiment (experiment: DB-03) performed by Sheets et al. (2007) and analyzed by Sheets et al. (2007), Straub et al. (2009), Hajek et al. (2010) and Ganti et al. (2011), there have been no experiments that monitor topography at a temporal resolution necessary to quantify individual channel dynamics and relate these dynamics to the stratigraphic architecture they produce.

In order to examine the dependence of time scale of measurement on the strength of compensation, we conducted an experiment, Tulane Delta Basin 10-1, (TDB 10-1). The TDB 10-1 experiment was modeled on the DB-03 experiment detailed in Sheets et al. (2007), but had the added aim of generating a stratigraphic package 2-3 times thicker than the DB-03 experiment, thus improving our ability to characterize compensation over a wider spectrum of temporal and spatial scales. The TDB 10-1 experiment was performed in the Delta Basin at Tulane University's Sediment Dynamics Laboratory (Figure 5). This basin is 2.8 m wide by 4.2 m long and 0.65 m deep. Accommodation is created by slowly increasing base-level using a motorized weir that is in hydraulic communication with the basin. This system allows base-level control through a computer interface with sub millimeter-scale resolution. Water and sediment supply to the Tulane Delta Basin are also controlled through the above mentioned computer interface. Water supply is controlled by a variable speed centrifugal pump, while sediment is delivered to the basin via an AccuFeed Vibra Screw Composite Feeder. The experiment included an initial buildout phase in which sediment and water were mixed in a funnel and fed from a single point source at the center of the upstream wall. The sediment feed rate was 0.011 L/sec, the water discharge was 0.451 L/sec, and their rates were kept constant throughout the experiment. As such, the ratio of water discharge to sediment discharge in this experiment was 41:1. It is important to note that the ratio of water discharge to sediment discharge does not always stay constant for natural systems. In natural basins these parameters vary over many time scales that could confound the interpretation for both allogenic and autogenic signals. For example, larger water discharge rates explicitly change the allogenic forcings, but also make larger channels and therefore alter the time scales of autogenic dynamics. The delta was allowed to prograde into the basin producing a symmetrical fluvial system that covered the width of the basin. After the system prograded 3.1 m from source to shoreline, base-level rise was initiated at a rate equal to the total sediment discharge divided by the desired delta area top (base-level rise rate = 5 mm/hr). This combination of sediment feed rate and base-level rise allowed the shoreline to be maintained at an approximately constant location through the course of the experiment. The sediment mixture was composed of 70% by volume quartz sand (Mean grain size D_{50} = 110 μm) and 30% coal sand (Mean grain size D_{50} =440 μm). The coal has a specific gravity of 1.3, whereas quartz has a specific gravity of 2.65, so the coal grains are substantially more mobile than the quartz grains and serve as a proxy for fine-grained clastics. The mixture of quartz and coal is similar to that used in previous experiments (Heller et al., 2001; Sheets et al., 2002; Martin et al., 2009b).

In order to visualize the active channel network, the input water was dyed with a commercially available blue food coloring and made opaque by adding a small amount of titanium dioxide. Finally, the edges of the basin were artificially roughened, in order to direct the channels away from the basin walls.

Three types of data were collected from the experiment: system morphology, surface topography, and deposit stratigraphy. The morphology of the fluvial system was recorded with two G10 Cannon cameras connected to a computer interface. One of the cameras (Camera 1) was positioned to collect images of the entire basin, which were used to characterize surface dynamics, while the second camera (Camera 2) was positioned to collect both surface morphology and topography data. Cameras 1 and 2 recorded images of the active delta top at 1 minute intervals. Topographic measurements were taken in a manner modeled on the XES subaerial laser topography scanner (Sheets et al., 2007). In contrast to XES, however, where the topography of the entire fluvial surface is recorded periodically, we chose to monitor the topography at 2 minute intervals along three flow-perpendicular transects, located 1.6 m, 2.1 m, and 2.6 m from the infeed point. This system uses oblique digital images of lines cast by vertical laser sheets from which true topography can be calculated. To measure a full cross-section of topography, including areas inundated by water, the experiment was stopped every two minutes and water was allowed to drain off the fluvial surface prior to collecting measurements. This arrangement allowed instantaneous (the exposure time of the camera) measurements, rather than the 30 to 45 minutes required for a full-surface scan. With this system, we obtained measurements with a horizontal spacing of ~1 mm and a vertical resolution of 0.5 mm. The TDB 10-1 experiment was run for 82 hours, and produced an average of 415 mm of stratigraphy. We sectioned, peeled, and imaged the deposit at each of the topographic strike-transects. Image data for all three data types were obtained using Cameras 1 and 2 that were mounted continuously in the same positions, meaning that a given pixel location in any one image corresponds to the same physical location in all three. We could locate a feature on a morphology image, match it with the elevation data from the same point on the corresponding topography image, and match both with the same point on the deposit image.

In order to examine the influence of the ratio of transport system size to basin size on the degree of stratigraphic organization a second experiment, TDB 10-2, was performed. The design of the TDB 10-2 experiment and data collection routine was identical to TDB 10-1 with the exception of the following parameters. TDB 10-2 was designed with a transport system that was twice the size of TDB 10-1. To accomplish this, the water and sediment discharge rates into the basin were doubled with respect to TDB 10-1. To maintain a constant shoreline location during the experiment the rate of base-level rise was also doubled relative to TDB 10-1. Table 1 details the key experimental variables in the two experiments.

No attempt was made to formally up-scale the results from this experiment to field scale. In addition, parameters associated with this experiment were not set to produce an analogue to any particular field fan-delta system. As such, specific geometric data associated with this experiment cannot strictly be utilized to estimate the field scale deposit geometries or dynamics of a specific system. Rather, the goal of the experiment was to create a self-organized, distributary depositional system in which many of the processes characteristic of larger fan-delta systems could be monitored in detail over spatial and temporal scales which are impossible to obtain in the field. This experimental technique is similar to the ‘similarity of process’ philosophy outlined in Hooke (1968) and expanded upon by Paola et al. (2009). Thus, the focus in this thesis is on identifying the general scales of compensation which characterize the evolution of topography in the TDB 10-1 experiment.

Chapter 5: EXPERIMENTAL RESULTS

5.1 General Observations

Utilizing the experimental setup discussed in the previous section and the experimental parameters summarized in Table 1, we constructed two self-organized fluviodeltaic deposits. As discussed in Sheets et al. (2007), the relatively high sediment to water discharge ratio (1:41) utilized in our experiments resulted in a fan-delta with a relatively high surface slope. This high surface slope leads to channelized flows that alternated between supercritical and subcritical Froude numbers. Froude number can be thought of as the ratio of potential energy to kinetic energy and describe different flow regimes of open channel flow. The high Froude numbers resulted in the formation of scour points generated at zones of convergent flow and associated with hydraulic jumps. These scours tended to migrate upstream with time in a manner analogous to knickpoint erosion. Deposition then was associated with flow expansion immediately downstream of the scours. The concave-up channelized depositional bodies preserved in the final stratigraphy are largely a result of these migrating scours, while the accumulation of sheet-like deposits with basal surfaces lacking unconformities are in large part due to flow expansion. This dynamic quasi-equilibrium state on the fluvial surface roughly held the average fan-delta slope to 0.05 throughout the experiment.

5.2 TDB 10-1

5.2.1 Topographic evolution

Aggradation of the fan-delta was promoted during the TDB 10-1 experiment via a steady base-level rise with a rate of 5 mm/hr. This base level rise coupled with constant input supplies of water and sediment resulted in the aggradation of the fan-delta with little net-movement of the shoreline over the course of the experiment (Figure 6). Following 82 hours of base-level rise the entire fan-delta surface aggraded roughly 410 mm. Time-space maps of fan-delta topography for the course of the experiment at the three laser transects are presented in Figure 7 A-C and show a steady long term deposition rate. While the long-term deposit shape and deposition rate was set by the shape of the experimental basin and the imposed base-level rise rate, short-term deposition patterns and rates were extremely variable. Utilizing the topographic scans we generated time-space maps of accommodation space at the three laser transects. Within the context of this experiment, we define accommodation space as space available for deposition below the equilibrium graded profile of the transport system at any spatial location within the fan-delta. We estimated accommodation space for all available time-space pairs in the TDB 10-1 experiment by detrending the time-space topography maps for the imposed long-term deposition rate and average long-term cross-stream topography (Figure 7 D-F). In the time-space maps of accommodation, negative values represent available accommodation space (e.g. the topography at that space and time is lower than the graded profile for that location at that time) and positive values represent negative accommodation space (e.g. the topography at that time and space is higher than the graded profile for that location at that time). The time-space maps of accommodation at the three laser transects show that the basin filled via the accumulation of depositional (and erosional) events that were both discontinuous in time and space. The unsteady nature of deposition in time and space is undoubtedly influenced by the autogenic migration of channelized flow on the fan-delta top.

Utilizing the topographic scans and images of the active transport system we estimated properties of the hydraulic geometry of the TDB 10-1 fan-delta system. First we estimated the mean depths of channel features on the fan-delta top. We focused on the mean depths of channel features, as they represent the average surface roughness scales in our experiment and thus are needed for testing the validity of our hypothesis for what sets T_C (Equation 3). Assuming the mean channel depths are equal to the deviation scale of depositional and erosional events relative to long-term average accommodation formation, we estimated mean channel depths of 11.2 mm, 9.4 mm, and 7.7 mm at the proximal, medial and distal laser locations by using time-space information of accommodation. In addition, to comprehensively record the hydraulic geometry, we also observed maximum channel depths of 14 mm, 12 mm, and 10 mm at the proximal, medial, and distal laser locations (Figure 8).

Next we estimated the average wetted fraction, B_f, at the three laser transects. B_f is equal to the total wetted width of transport system divided by the total basin width. We use B_f as a proxy for channel widths as the high width to depth ratio of much of the experimental flows makes estimating channel widths difficult. We estimated B_f using our dataset of overhead images of the active transport system. Using a threshold blue luminosity value we separated dry regions on the delta top from wet regions, given that we dyed the input water blue. The threshold value used for this operation was picked by identifying a value that on visual inspection appeared to correctly separate the two regions (Figure 9). Using the binary images we calculated the fraction of cross-basin length that was inundated with water for each image and then calculated the mean wetted fraction at each laser transect.

5.2.2 Experimental strata

After 82 hrs of aggradation in the TDB 10-1 experiment, pseudo sea level was slowly lowered and the delta basin drained. Following a drying phase, the experimental deposit was vertically sectioned at the three laser transects in order to observe the final deposit stratigraphy (Figures 10-12). Additionally, synthetic stratigraphy was generated from the measured transects of topography. The synthetic stratigraphy is created from stacked delta-top profiles with topography clipped to account for sediment removed during erosional events (Martin, 2007; Figures 10-12).

Utilizing the physical and synthetic stratigraphy at the three laser transects we have made the following stratigraphic observations. First, the strata at the three transects primarily consist of two facies: incisional channel-fill structures and tabular sheets (Figures 10-12). In contrast to laterally constrained high-curvature channel bodies, the sheet-like deposits are laterally extensive low-curvature features. Next we see a decrease in the number of channel bodies preserved from the proximal to distal measurement transect in addition to a decrease in the width and depth of preserved channels from source to sink. Finally, we see a decrease in the percent of quartz sediment in the stratigraphy and an increase in the percent of coal as we move from the proximal to distal transects.

5.2.3 Decay of σ_{ss} with increasing time interval

Utilizing the digital topographic dataset for the TDB 10-1 experiment, we calculated σ_{ss} (Eq. 1) at each topographic transect for every possible pairwise combination of topographic surveys, allowing us to define the decay of σ_{ss} over time windows of 2 – 1000 minutes (Figure 13 A-C). Similar to our observation of the decay of σ_{ss} in our numerical model we observe that the strength of compensation as quantified by κ is scale dependent. For short time windows the magnitude of κ at the three measurement locations is less (κ = 0.66, 0.57, and 0.56 for the proximal, medial, and distal transects, respectively) than the magnitude of κ measured for long time windows (κ ~ 1.0). During the experiment the maximum roughness on the transport system was associated with channels. As such we calculate T_C with Equation 3, where l represents the mean depth of channels along a given transect as reported in Section 5.2.1. This process resulted in predictions of T_C between 92 and 134 min. These T_C predictions are in good agreement with the location of sharp inflections in the plots of σ_{ss} as a function of T (Figure 13 A-C). Finally, we note a decrease in the estimated short-term κ values (κ below T_C) and observed T_C from the proximal to distal transect.

5.2.4 Stratigraphic Organization in Time vs. Thickness

The degree of age control associated with natural basins is always less than what can be achieved in lab experiments. The compensation index proposed by Straub et al. (2009) is constructed using plots of σ_{ss} against measurement window in time. Here we demonstrate that the measurement window can also be spatial, namely the average deposit thickness between two stratigraphic surfaces. Comparison of σ_{ss} for this experiment shows a good match between κ calculated in time and space (Figure 14). This indicates that stratigraphic horizons may be used in place of timelines for analysis of deposits lacking adequate age control.

5.3 TDB 10-2

5.3.1 Topographic evolution

The topographic evolution of the distributive fluvial deltaic system constructed in the TDB 10-2 experiment is in many ways similar to the topographic evolution of TDB 10-1. The most pronounced difference between the two experiments, however, was the enhanced rates of system evolution in TDB 10-2 associated with the doubling of Q_w, Q_s, and $\bar{r}$ in TDB 10-2 relative to TDB 10-1 (Table 1). Aggradation of the fan-delta was promoted during the TDB 10-2 experiment via a steady base-level rise with a rate of 10 mm/hr. This base level rise coupled with constant input supplies of water and sediment resulted in the aggradation of the fan-delta with little net-movement of the shoreline over the course of the experiment (Figure 15). Following 40 hours of base-level rise the entire fan-delta aggraded roughly 401 mm. Time-space maps of fan-delta topography for the course of the experiment at the three laser transects are presented in Figure 16 A-C and show a steady long term deposition rate. Similar to TDB 10-1, accommodation space in the TDB 10-2 experiment was filled via punctuated (non-steady in time and space) depositional and erosional events. This punctuated evolution can be seen in the structure of the time-space maps of accommodation shown in Figure 16 D-F.

The hydraulic geometry of the sediment transport system in TDB 10-2 expanded relative to TDB 10-1 owing to the doubling of Q_w and Q_s. Similar to TDB 10-1 we utilized the digital accommodation data and images of the active transport system to quantify the mean channel depths and wetted fractions, respectively at each of the three measurement transects. The mean channel depths, estimated by the deviation scale of depositional and erosional events relative to long-term average accommodation formation, were 11.7 mm, 11.8 mm, and 8.8 mm respectively at proximal, medial and distal transects. Meanwhile, the maximum channel depths recorded at these locations were 26 mm, 22 mm and 19 mm respectively (Figure 17). The mean wetted fractions at the proximal, medial, and distal transects, used as a dimensionless proxy for channel width (Kim and Paola, 2007; Kim and Jerolmack, 2008), were 0.63, 0.63 and 0.72, respectively. These measurements indicate that the hydraulic geometry increased in TDB 10-2 relative to TDB 10-1 due to the increase in water and sediment feed rates (Table 2).

5.3.2 Resulting experimental strata

Similar to the topographic evolution of our two experiments, the stratigraphy of TDB 10-2 is in many ways similar to the stratigraphy of TDB 10-1. The most pronounced difference in the stratigraphy of TDB 10-2 relative to TDB 10-1 is the size of the preserved channel bodies in the two experiments. In Figures 18-20 we present the physical and synthetic stratigraphy for the proximal, medial, and distal transects, respectively. We note a striking increase in the widths of preserved channel bodies in the TDB 10-2 experiment relative to the TDB 10-1 experiment. There are a few channel-form structures with relatively large depths, but based on the comparison of mean channel depths in two experiments, we ascertain that these channels are scoured by individual high-magnitude flow events such as hydraulic jumps. Overall the mean channel aspect ratios of TDB 10-2 increase dramatically compared to TDB 10-1.

5.3.3 Decay of σ_{ss} with increasing time interval

Utilizing the same process outlined in Section 5.2.3, we calculate σ_{ss} (Eq. 1) at each topographic transect for every possible pairwise combination of topographic surveys. Similar to our observations for the TDB 10-1 experiment, we observe a scale-dependent decay of σ_{ss}, the variability of sedimentation to subsidence, as a function of T (Figure 21 A-C). For all three transect locations, two identifiable linear regimes are observed in the decay of σ_{ss} with time. Within short-time windows, the decay of σ_{ss} at proximal, medial and distal transects is characterized by κ values of 0.63, 0.61, and 0.58, respectively. Over long-time windows, the decay of σ_{ss} is characterized by a κ value of 1.0 at each of the three transects.

We calculate compensation time scale, T_C, with equation 3, with l equal to the mean depth of channels at each of the transect locations. This process resulted in predictions of T_C between 53 and 71 min. Again, we note that these T_C predictions are in good agreement with the location of sharp inflections in the plots of σ_{ss} as a function of T (Figure 21 A-C). Similar to TDB 10-1, we note a decrease in the estimated short-term κ values (κ below T_C) and observed T_C from the proximal to distal transect.

Finally, using our estimated channel depths and imposed base level rise rates we note that Eq.3 yields different T_C predictions for the two experiments at each of the measurement locations (Table 2) and that these predictions match the observed location of scale breaks in the decay of σ_{ss} with T. Conversely, we observed little difference in κ below T_C for the two experiments at each of the measurement locations (Table 2). This occurs despite the strong difference in B_f of the two experiments at each of the transect locations. In Figure 22 we merge plots of the decay of σ_{ss} with T both in dimensional and non-dimensional time space in order to compare TDB 10-1 and TDB 10-2. The power-law relationship between σ_{ss} and non-dimensionalized time is expressed as:

$$\sigma_{ss} = a(T/Tc)^{-\kappa} \quad (4)$$

where the ratio T/T_c denotes a non-dimensionalized time T^*, as used in Fig. 22. The similarity of κ and difference in T_C for the two experiments at each transect location is discussed in Section 6.

5.4 Scale-dependent compensation in field stratigraphy

Previous studies that investigated the decay of σ_{ss} with scale examined either experimental systems or stratigraphy imaged in industry-grade seismic data (Sheets et al., 2002; Lyons, 2004; Straub et al., 2009). Unfortunately, industry-grade seismic data resolution is such that σ_{ss} cannot be measured for deposits with mean thicknesses less than ~20 m, a thickness of similar magnitude to many channel depths. Owing to this limited resolution, a scale-dependence in compensation set by channel dynamics cannot be examined with these field data sets. To avoid the sampling problem and investigate scale-dependent stacking patterns in field stratigraphy, we use an outcrop-based study where stratigraphic architecture can be mapped above and below the scale of individual channel bodies.

The Upper Cretaceous/Paleogene Ferris Formation was deposited by a rapidly aggrading fluvial system in southeast Wyoming during the early Laramide Orogeny (Eberle and Lillegraven, 1998). In the study area the Ferris Formation dips at ~80° S exposing a basin cross-section nearly orthogonal to paleoflow direction. The unit exhibits well-developed stratigraphic organization (Figure 23) where clusters of closely spaced channel bodies are separated from each other by mudstone-dominated intervals. This clustered pattern is observable throughout the outcrop belt, which extends several kilometers beyond the mapped study area.

Channel bodies mapped in the field are between 1 to 10 m thick and can be tracked laterally into their contemporaneous floodplain deposits.

The distribution of channel deposits at this field site was shown to be statistically clustered (Hajek et al., 2010). No evidence for external controls on the spacing of channels were found within the outcrop (Hajek, 2009), and this pattern is interpreted to indicate autogenic avulsion behavior, similar to that found by Jerolmack and Paola (2007). To quantify the decay of σ_{ss} for the Ferris Formation, stratigraphic horizons which we infer as pseudo time horizons were mapped based on the stratigraphic order of channels (Figure 23 E). These horizons track the basal scour surfaces of channels up the flanks of channel bodies and extend laterally into presumed contemporaneous floodplain deposits. As seen in the model and experiment, σ_{ss} vs. stratigraphic thickness calculated for this dataset shows two regimes where: 1) κ steadily increases from a value of 0.5 to 1.0 and 2) κ is constant and equal to 1.0 (Figure 24). We note that the transition to pure compensation is complete for basin-wide deposits with mean thicknesses in excess of 40 m. It is worth noting that this thickness is 4 times greater than the maximum thickness of channel bodies at this site.

Chapter 6: DISCUSSION

Development of models for the architecture of channelized fluvial stratigraphy is vital for correctly interpreting 3D seismic data and correlating strata from well logs in alluvial basins. This architecture can display varying degrees of stratigraphic order depending on depositional environments and allogenic forcings. We recognize two geometric families of stratigraphic organization: (1) compensational stacking (Straub et al., 2009) and (2) anti-compensation leading to channel clustering Hajek et al., (2010). At present, a full understanding of the time and space scales associated with these two families of stratigraphic organization are poorly understood. In addition, the majority of studies into stratigraphic organization have focused on allogenic forcings and their stratigraphic products (Samuel, et al., 2003; Schwab et al., 2007; Hofmann et al., 2011), with few exceptions (Jerolmack and Paola, 2007; Hajek, et al., 2010). In this study, we have shown that sediment transport systems experiencing steady allogenic forcings can produce stratigraphy with non-random organization which can be measured over long time and space scales. Below we focus on three aspects of this stratigraphic organization: (1) The dependence of κ on the time scale of measurement, (2) the influence of the ratio of transport system size to basin size on κ, and (3) the change in stratigraphic organization observed from sediment source to sink in alluvial basins. Finally, we discuss several outstanding questions related to stratigraphic organization.

6.1 Scale-dependent compensational stacking

In the experimental and field basins analyzed in this study we find that the strength of compensation is scale dependent (Figures 13, 21, 24). For all cases studied κ increases with stratigraphic scale until saturating at a value of 1.0. In the laboratory experiments, where we can link surface dynamics directly to the architecture of preserved stratigraphy, the time scale at which these systems transition to pure compensation (κ = 1.0) is correctly predicted by Equation 3. This result has implications for stratigraphic architecture and our ability to invert stratigraphy for paleo-environmental conditions.

Equation 3 essentially states that the geometry of deposits carries the signature of stochastic autogenic dynamics out to a time scale equal to the time necessary to fill a basin to a depth equal to the amount of surface roughness in a transport system. Interestingly, T_C for many systems extends into time scales commonly associated with large-scale allogenic cycles (e.g., Milankovitch cycles). For example, we calculate T_C for the Lower Mississippi Delta. We assume that the roughness length scale in Equation 3 is well approximated by mean channel depth for lowland deltas. Using a channel depth for the Lower Mississippi River of 30 m and a subsidence rate of 0.23 m/kyr estimated for the last 8 Myrs (Straub et al., 2009) we calculate a T_C of 130,000 yrs. This duration is significantly longer than the period of the Earth's eccentricity (100,000 yrs), inclination (70,000 yrs), obliquity (41,000 yrs), axial precession (26,000 yrs), or apsidal precession (21,000 yr

s) cycles. These Milankovitch cycles impact the amount and distribution of solar radiation entering the atmosphere, specifically the amount of solar radiation entering the atmosphere during summer months at high latitudes. The current configuration of continents is associated with a great amount of land at high latitudes. As the specific heat of most solids are generally lower than that of water, land masses respond to temperature change more quickly than oceans. As a result, changes in the length or intensity of high latitude summers strongly influence the size of high latitude glaciers. Changes in the amount of water stored in these glaciers directly impact the sediment supply and global eustasy which are commonly discussed allogenic forcings.

In addition to climate cycles and their influence on global eustasy, it is also important to note that the time scale of compensation for many sedimentary systems overlaps many commonly discussed tectonic time scales. For example, it has been hypothesized that earthquakes cluster in time on some fault systems (Prosser, 1993; Dorsey et al., 1997; Gupta et al., 1998; Gagliano, 2005). This earthquake clustering would result in long-time periods with little or no movement along a fault section (and thus little generation of accommodation space along normally faulted basins experiencing constant eustasy) followed by periods of rapid movement a fault system and thus rapid changes in accommodation space. Much of the evidence supporting these earthquake clusters has come from the interpretation of cyclicity in stratigraphic patterns that are assumed to record allogenic forcings. For example Dorsey et al., (1997) used cyclicity in stratigraphic architecture of Pliocene Gilbert-type delta in the Loreto basin, Baja California Sur, Mexico to argue for earthquake clustering with frequencies between 300 – 40,000 yrs. Additional studies in the Dead Sea graben and Xiaojiang fault zone of China suggest tectonic cycles with periods of 20,000~30,000 yrs (Marco et al., 1996; Xu and Deng, 1996). Coupled with climatic cycles, the subsidence cycles composed of relatively active and quiescent intervals would further complicate the interpretation of allogenic forcings in the sedimentary record. In addition, the spatially and temporally variable movement of subsurface tectonic systems could also cause complex autogenic responses and potentially further prolong compensation time scales due to the additional surface roughness that they impart on transport systems. Apart from the intermingling of T_C and allogenic cycles, we also note my T_C estimate for the Mississippi Delta is long in comparison to other previously discussed autogenic time scales for the Mississippi Delta. For example my T_C estimate is roughly 100 times greater than the ~1,300 yr reoccurrence interval for large avulsions of the Lower Mississippi River predicted by Reitz et al. (2010) and estimated from field data by Aslan et al. (2005).

These examples highlight the large amount of time necessary for autogenic surface-process dynamics to average out in the stratigraphic record. The intermingling of T_C with time scales associated with some large-scale allogenic cycles presents a challenge to sedimentologists when interpreting paleo-environmental records preserved in stratigraphy. T_C provides an estimate of temporal or spatial scales below which stratigraphers should be wary about interpreting allogenic signals.

Analysis of two end-member scenarios for Equation 3 provides further insight into the time scales associated with autogenic compensation in stratigraphic basins. The first end-member scenario is one in which a basin is tectonically stable and thus experiencing no long-term subsidence or aggradation. While this scenario is associated with no long-term aggradation, all transport systems experience autogenic processes which lead to short time scale deposition and erosion events (Paola and Borgman, 1991; Kim and Jerolmack, 2008). In this scenario all deposits will carry a signature of stochastic autogenic dynamics as Equation 3 would predict $T_C = \infty$. The second scenario involves stratigraphy constructed from an unconfined transport system, for example deep-water lobes constructed by unconfined turbidity currents (Pirmez et al., 2000; Pyles, 2007). In this scenario channel depth is zero and thus T_C is equal to zero. As a result, these systems can respond to allogenic forcings through compensation instantaneously.

In our laboratory experiments the appropriate scale of surface roughness in our T_C formulation was identified as the mean depth of the systems' channels. We hypothesize that channel depth is the appropriate length scale to use when estimating T_C for systems where the avulsion cycle is the lowest frequency autogenic process. Recent studies have identified autogenic processes that happen over time scales significantly longer than the avulsion cycle. Examples include autogenic lake formation and filling (Kim and Paola, 2007) and channel belt clustering (Jerolmack and Paola, 2007; Hajek et al., 2010). These long-period autogenic dynamics appear to occur in environments with strong tectonic forcing and/or significant sediment cohesion. We predict that these newly identified autogenic dynamics result in surface roughness scales that exceed the depth of a system's channels and thus could result in T_C values that further overlap some long-period allogenic forcings. Thus solving Eq. 3 with a roughness length scale equal to mean channel depth results in a minimum estimate of T_C. This hypothesis likely explains why pure compensation was only observed beyond stratigraphic scales 4 times the measured sand-body thickness in the Ferris outcrop stratigraphy described in Section 5.4.

6.2 The size of depositional system relative to basin size

The experiment TDB 10-2 was performed to examine whether the size of a sediment transport system relative to the size of the basin it fills influences the architecture and organization of stratigraphy. TDB 10-2 was designed to aggrade at twice the speed of TDB 10-1 via doubling Q_w, Q_s, and the rate of base-level rise. A comparison of the resulting surface dynamics and stratigraphy is given in Table 2. This data illustrates that while the mean channel aspect ratios of the transport system in TDB 10-2 were greater than TDB 10-1, κ at the three measurement transects was not different to a statistically significant degree. We will discuss the two autogenic parameters, κ and T_C and their dependence (or lack thereof) on the size of the experimental transport system relative to the size of the experimental basin separately, starting with T_C. At the three measurement transects the increase of Q_s and Q_w in TDB 10-2 relative to TDB 10-1 resulted in intensified hydraulic scours, producing a near doubling of maximum channel depths in TDB 10-2 relative to TDB

10-1. However, the delta roughness lengths of TDB 10-2 estimated by mean channel depths remain similar or slightly large relative to TDB 10-1. The relatively small increase in channel depths, in addition to the 2x rate of base-level rise in TDB 10-2 relative to TDB 10-1 resulted in different amounts of time necessary for aggradation of stratigraphic packages with equivalent thicknesses to the experimental channel depths. This result complies with theory developed by Parker et al. (1998) which predicts that systems with equivalent ratios of Q_s:Q_w will have equivalent channel depths. This theory also predicts that a doubling of both Q_s and Q_w results in a doubling of channel widths. For systems well approximated by the theory of Parker et al. (1998) we would expect a linear decrease in T_C as the absolute magnitudes of Q_s and Q_w increases, so long as the ratio of Q_s:Q_w remains constant. Consequently, it is not surprising to observe a decrease in T_C of a factor of roughly 2 for the TDB 10-2 experiment relative to TDB-10-1. In addition to this theoretical estimate, the comparison of experimental results in both dimensional and dimensionless time space (Figure 22) also give us confidence to conclude the system with a larger transport system size, namely TDB 10-2, appears to transition to purely compensational stratigraphy (κ = 1.0) over shorter time scales than systems with smaller ratios of transport system size to basin size.

Next, we observe that at the three measurement transects the estimated values for κ below T_C are near identical in the two experiments. This result suggests that for systems with equivalent environmental and transport parameters (i.e. grain size distributions, ratio of Q_s:Q_w, etc.) the size of the transport system relative to the size of the basin does not influence stratigraphic organization. As a result, while the absolute dimensions of channel bodies and sheet deposits preserved in stratigraphy are influenced by the absolute size of a transport system, the organization of these deposits relative to one another is unaffected. This observation is consistent with the experimental work of Strong et al. (2005) who found that the most important parameter influencing the density of channel bodies and local grain size is the location of a stratigraphic section within a mass-balance framework.

6.3 Sediment source to sink decay of κ

While the estimated values of κ at each of the three measurement locations are similar in the TDB 10-1 and TDB 10-2 experiments, both experiments are characterized by a downstream decay in κ. To further investigate the decay of κ from sediment source to sink we analyze data collected from an experiment, DB-03, conducted with constant allogenic forcings conducted in the Delta Basin at St. Anthony Falls Laboratory at the University of Minnesota (Sheets et al., 2007). The allogenic forcings in the DB-03 experiment, including Q_s, Q_w and the rate of base-level rise were identical to TDB 10-1. Further, topography in this experiment was collected along three measurement transects located perpendicular to the dominant flow direction every 2 minutes at proximal, medial, and distal locations.

Utilizing the time-space elevation data from the three DB-03 measurement transects (Figure 25) we characterize the decay of σ_{ss} with time utilizing the same techniques outlined in Section 4. Similar to TDB 10-1 and TDB 10-2 we observe a time-scale dependence for κ at each measurement location and a decrease in κ

measured below T_C from the proximal to distal measurement transects (Figure 26).

One important difference between DB-03 and the experiments conducted in the Tulane Delta Basin is the geometry of the experimental basin and the shape of the resulting delta. The DB-03 experiment included an initial build out phase in which sediment and water were mixed in a funnel and fed into one corner of the basin while base-level remained constant. The delta was allowed to prograde into the basin and produced an approximately radially symmetrical fluvial system. After the system prograded 2.5 m from source to shoreline a base-level rise was initiated. The radially symmetric geometry differs significantly from the experimental geometry of the Tulane Delta Basin (Figure 27). Further, the total length of the DB-03 depositional system (2.5 m) was less than the TDB 10-1 and TDB 10-2 depositional systems (3.1 m). Given these geometric differences it is difficult to discuss the organization of the DB-03 stratigraphy relative to the stratigraphy of the experiments conducted in the Tulane Delta Basin in a reference framework defined by the absolute distance from the sediment infeed point. In order to quantitatively compare the decay of κ with distance along a transport system we map the downstream distance (x) for each measurement transect into a fraction of sediment supplied to a basin deposited upstream of a transect of interest. This mass-balance framework, first proposed by Strong et al. (2005) utilizes a non-dimensional number $\chi(x,)$ where (x) is equal to the fraction of all supplied sediment deposited between the sediment source at x=0 and a distance x downstream. Formally, $\chi(x)$ is defined by:

$$\chi(x) = \frac{\int_0^x r_{\Delta T}(x)dx}{\int_0^L r_{\Delta T}(x)dx} \qquad (5)$$

where $r_{\Delta T}(x)$ denotes sedimentation rate at a given downstream distance x measured over a time interval ΔT, L is the total length of the depositional system.

After mapping all measurement transects locations into a mass-balance framework, we are able to compare the estimated κ values below T_C in three experimental data sets (Figure 28). We find that within a mass-balance framework a similar absolute trend in decay of κ (and thus stratigraphic organization) with $\chi(x)$ is found in all three data sets. At present we do not fully understand the morphodynamics that result in the downstream decay of stratigraphic organization, and have not analyzed any field data sets to see if this trend can be observed in field scale stratigraphy. However, several characteristics of the topographic evolution of our experiments might be associated with the observed decay of κ from sediment source to sink. These include a change in the variance of deposition rate from source to sink. We observe higher variability in deposition rates at the proximal relative to distal measurement transect in all experiments. In additional parameter that might influence the decay of κ from sediment source to sink is the degree of channel confinement. In proximal locations flow in my experiments shows a higher degree of channel confinement than distal locations. This results in the construction of stratigraphy with a high density of channel bodies relative to lobe deposits in proximal vs. distal locations. Regardless of the exact morphodynamics, my findings predict a reduction of stratigraphic organization, as manifest through compensation, from source to sink in alluvial basins.

Chapter 7: FUTURE RESEARCH DIRECTION

Compensational stacking describes the stratigraphic architecture of offset depositional bodies. As discussed in the work of Stow and Johansson (2000) and Deptuck et al. (2008), compensational stacking can be observed on a range of scales from the amalgamation of beds to the offset of channels and channel complexes. The degree of lateral offset associated with the depocenters can be much smaller, though, for compensation at the bed scale relative to the channel-complex scale. This suggests that our estimate of κ might be dependent on the width of a measurement transect relative to the total width of a basin. This question can likely be addressed through future analysis of our experimental data.

At present we do not fully understand the linkage between avulsion time scales and mechanics and κ. Several authors have noted that the frequency of avulsions is influenced by the long term rate of aggradation in alluvial basins (Tornqvist and Bridge, 2002; Martin et al., 2009a). Thus a system undergoing pure progradation would have a low avulsion frequency compared to a similar system undergoing pure aggradation. As avulsion is a key process in the migration of depocenters in alluvial basins, κ is likely a function of avulsion frequency and needs to be further examined. In addition, several authors have shown that avulsion frequency is also influenced by the rate of in-channel deposition relative to flood plain deposition (Tornqvist and Bridge, 2002; Jerolmack and Paola, 2007). As such, the processes associated with flood plain deposition likely influence the magnitude of κ.

The examination of stratigraphic organization in this work has focused on environments experiencing constant allogenic forcings resulting in the pure aggradation of sedimentary deposits. While we believe that it is best to characterize the morphodynamics of deltas in environments experiencing constant allogenic forcings prior to examination of non-linear forcings, at some point non-steady allogenic forcings must be examined. It is well documented that changes in boundary conditions can cause short-term variability in sediment transport rates in sedimentary basins (Van Wagoner; 1995; Perlmutter et al., 1998; Kim et al., 2006). Examples of this include stratigraphic models where changes in climate or base level influence volumes of sediment stored in terrestrial and marine environments. We expect that κ is influenced by allogenic variability in sediment transport rates, but it is difficult at present to separate the signal of this variability from autogenic variability. Future work will undoubtedly need to focus on the quantitative signature of these allogenic forcings in the stratigraphic record and techniques to separate these forcings from autogenic stratigraphic product.

Chapter 8: CONCLUSION

Inherent characteristics of sedimentary systems are often thought to generate small-scale noise in the stratigraphic record and are usually ignored in stratigraphic interpretation (Mack and Rasmussen, 1984; Peper and Cloetingh, 1995; Van Wagoner, 1995; Martin et al., 2009b). However, autogenic dynamics can also occur over large temporal and spatial scales and construct deposits with sedimentary records that mimic stratigraphic signals presumed to result from changes in external boundary conditions. To address the scales and magnitude of autogenic fluctuations, in this thesis we utilize several methods to quantify autogenic processes and their stratigraphic products. We utilize surfaces statistics to quantify the decay in the variability of deposition rates relative to generation of accommodation space in alluvial basins. The rate of this decay, termed the compensation index, is used to quantify the strength of compensation and the time scales associated with autogenic processes. Analysis of stratigraphy generated from physical experiments, numerical modeling, and field outcrops, yields the following conclusions:

1) We derived the characteristic scale that measures the time required to average individual events into large scale stratigraphic packages with geometries set by long-term sediment supply and accommodation. Below this time scale, T_C, the geometry of deposits is partially set by stochastic autogenic dynamics of the transport system. The two parameters that control T_C are channel depth and the

long-term average aggradation rate. We note that estimates of T_C for many natural systems are of a similar magnitude to important low frequency climate, tectonic and/or sea-level changes. This fact likely complicates our ability to extract the record of these allogenic signals from stratigraphy; however quantitatively constraining the spatial or temporal limit of autogenic stratigraphy using κ and T_C will help determine when these signals are potentially compromised.

2) We find that the ratio of transport system size to basin size does not influence the organization of stratigraphy, assuming all other allogenic forcings (including the ratio of sediment to water flux) are held constant. In this thesis we discussed two experiments which we performed in Tulane Universities Delta Basin. These experiments had identical allogenic forcings with the exception that one experiment had twice the input water and sediment flux and twice the base level rise rate of the first experiment. While the increase in water and sediment discharge rates resulted in an increase in the width of channelized flows in TDB 10-2 relative to TDB 10-1, it did not significantly alter κ but impacted T_C due to near identical flow depths in the two experiments. As a result, while the stratigraphic building blocks, including channel and lobe deposits, were wider in TDB 10-2 relative to TDB 10-1, their organization relative to one another was not influenced but we would expect a deposits to compensationally stack within a smaller stratigraphic interval.

3) We observe a decay in stratigraphic organization, quantified through the

compensation index, from sediment source to sink in three laboratory experiments. These three laboratory experiments had the same ratio of water to sediment flux and similar input grain size distributions, but differed in the absolute magnitude of water and sediment flux, base-level rise rate and experimental geometry. However, following transformation of stratigraphic location into a mass balance coordinate system we found that all three experiments shared a similar absolute trend in the decay of stratigraphic organization from sediment source to sink. This observation suggests that a predictable relationship between stratigraphic organization and non-dimensional distance along a sediment transport system might exist and could be used to aid in the modeling and prediction of field-scale stratigraphic architecture.

FIGURES

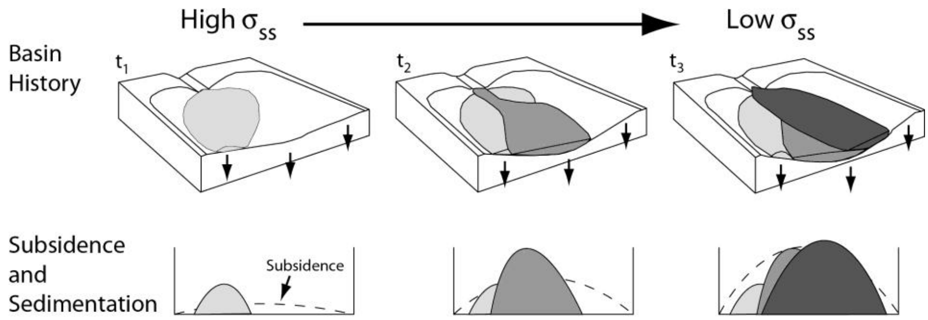

A)

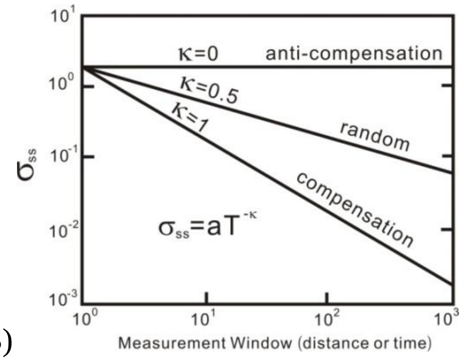

B)

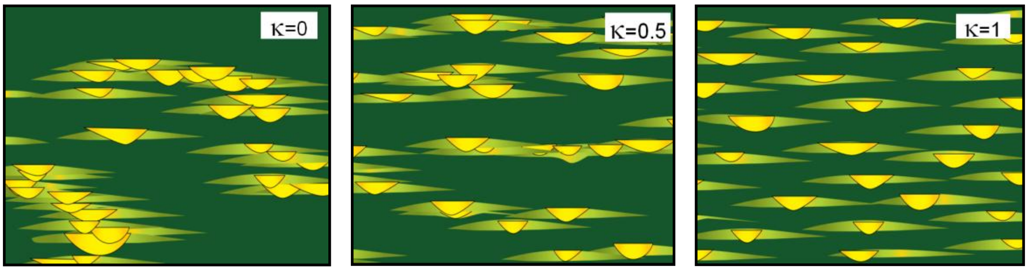

C)

Figure 1: A) Schematic from Lyons (2004) describing the progression of a basin towards equilibrium. The balance between sedimentation and subsidence in a basin improves over time. In the block diagrams illustrating basin history, subsidence (indicated by arrows) is temporally constant but spatially variable. Sedimentation, represented by lobes of different color, is both temporally and spatially variable. The balance between sedimentation and subsidence for an arbitrary cross section at the three time steps is represented graphically below each block. At the earliest time, t_1, subsidence is small and sedimentation is local resulting in a poor fit between the two. However, as the basin develops, subsidence increases and the sedimentary system has an opportunity to occupy a larger fraction of the total area. The result then, at later times t_2 and t_3, is that the fit between sedimentation and subsidence improves. Taking the ratio of sedimentation over subsidence pointwise across the basin for each time step would produce ratio distributions with decreasing standard deviations over time. B) Illustration of decay of σ_{ss} in basins with perfect anti-compensation (κ = 0.0), no compensation (κ = 0.5), and perfect compensation (κ = 1.0). C) Schematic diagrams describing different channel stacking patterns and their relationship to different κ values. Channel-fill structures are marked by yellow color with light green levee deposits extending into dark green floodplain.

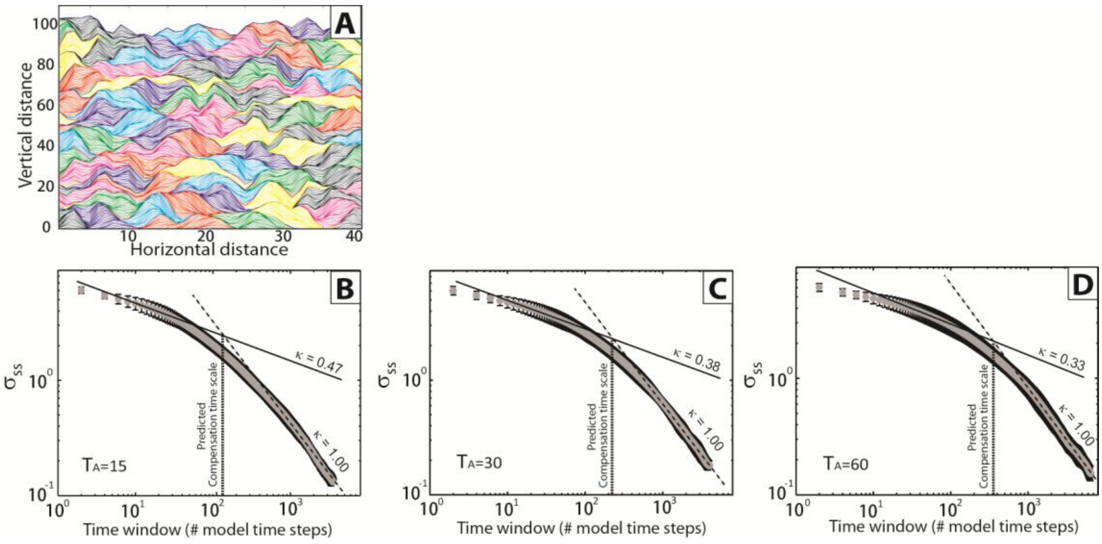

Figure 2: Numerical model stratigraphy and associated σ_{ss} decay with time. A) Output from object-based stacking model. Deposits of a single color represent deposition between avulsion events. In this model an avulsion occurs every 30 time steps. B-D) σ_{ss} vs. time plots based on models with different avulsion time scales. T_A denotes the avulsion time scale. These time scales determine the intervals during which deposit stacking is localized and hence result in corresponding roughness lengths (respectively 5, 9, 14 from plot B to plot D). On each plot, over short time scales depositional elements cluster to form anti-compensationally stacked deposits, while over long time intervals, above T_C, deposits stack in a purely compensational manner (see text). Error bars represent geometric standard deviation.

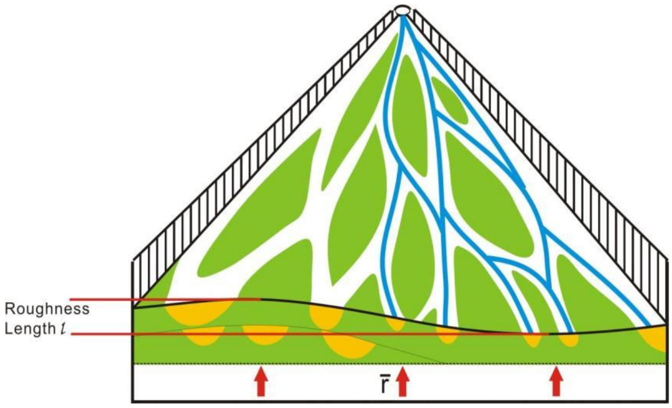

Figure 3: Schematic describing the parameters that influence the compensation time scale in deltaic environments. The maximum topography roughness is denoted by l while the basin-wide average long-term sedimentation rate is represented by $\bar{r}$. We hypothesize that the scale-break between deposit geometries that record $\kappa < 1$ and $\kappa = 1$ occurs at the time necessary to generate a deposit with a mean thickness equal to the maximum amount of roughness on the transport system.

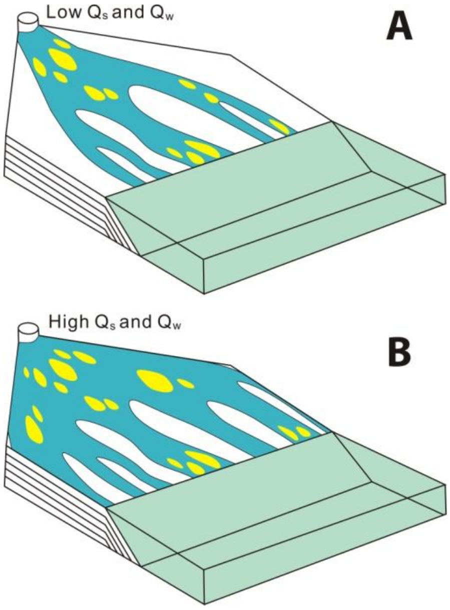

Figure 4: Schematic diagram describing difference in depositional systems with relatively high and low sediment and water discharges. A) A high ratio of Q_s:Q_w and weak sediment cohesion result in a sediment-rich braided channel network with multiple channels (Blue) and bars (yellow). In this scenario, relatively low absolute values for Q_s and Q_w result in a channel network with a low wetted fraction B_f) A laterally extensive braided channel network with high wetted width results from relatively high absolute values of Q_s and Q_w.

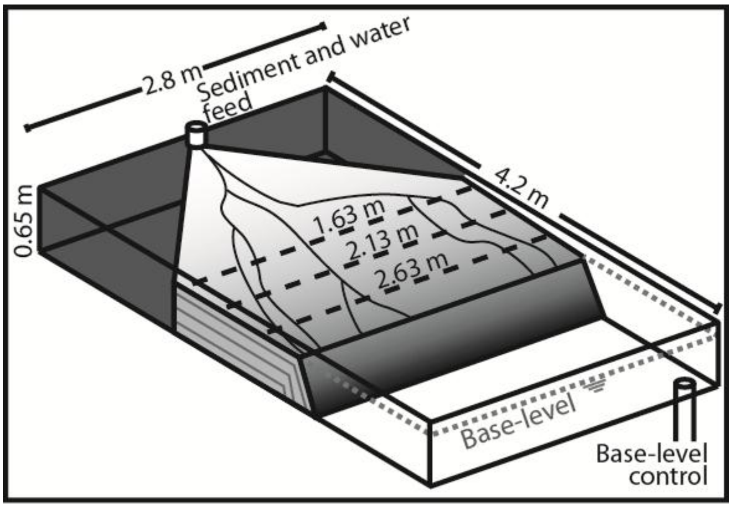

Figure 5: Schematic diagram of Tulane Delta Basin facility. Positions of proximal, medial and distal topographic transects in TDB 10-1 experiment are indicated by black dashed lines on fluvial surface. Note that base-level control is in opposite corner of basin from infeed point.

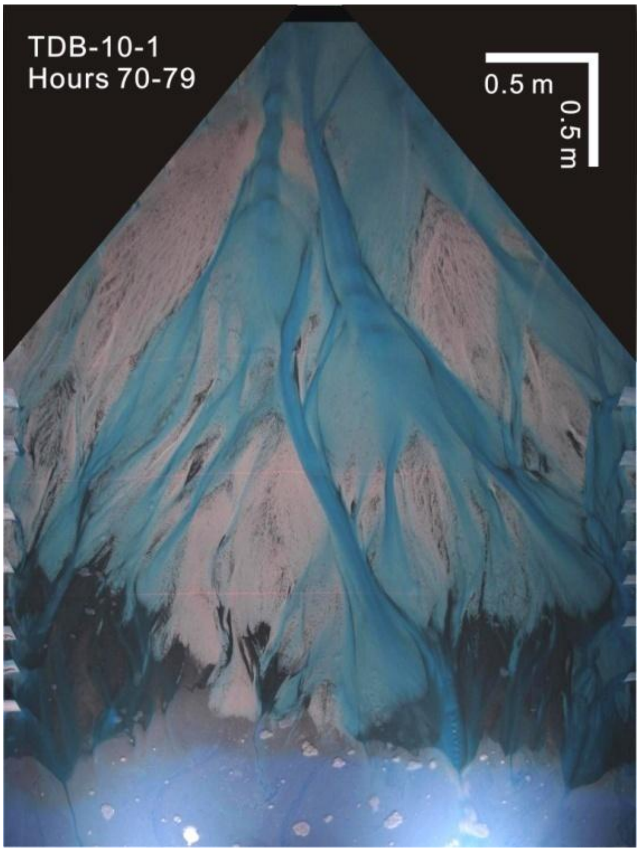

Figure 6: Overhead photograph taken at 76 hours into the aggradational phase of TDB 10-1 experiment. Flow is dyed blue to aid visualization. System is approximately 3.1 m in length from source to shoreline.

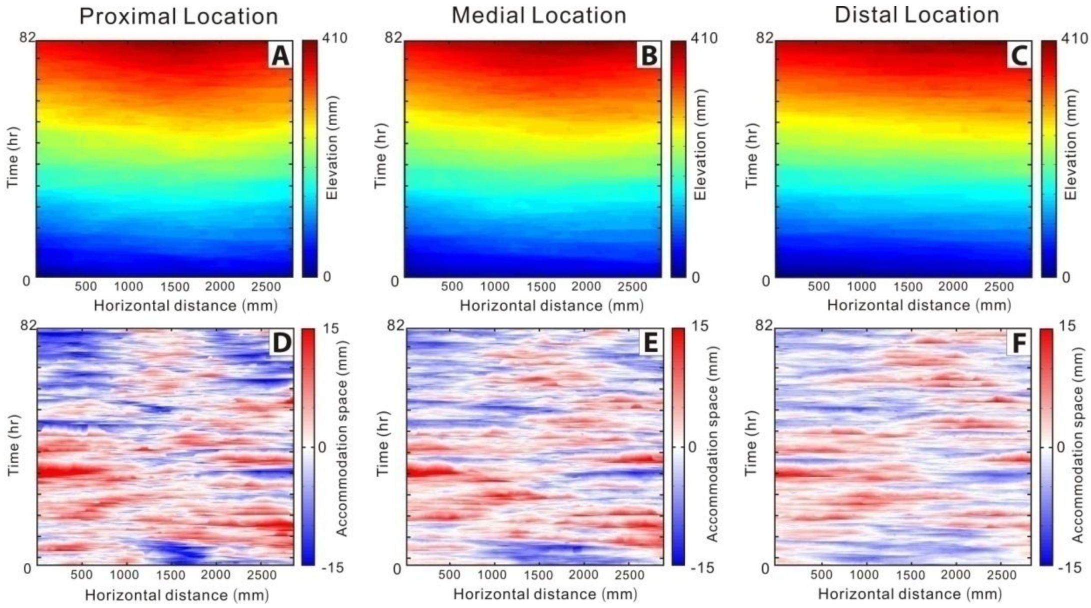

Figure 7: Data defining evolution of topography and surface dynamics for the TDB 10-1 experiment at the three measurement transects. A-C) Time-space plots of sequential delta-top profiles for the three measurement transects shown every 2 min for the course of the 82 hr experiment. D-F) Accommodation-space plots calculated from time-space data. Accommodation represents distance below long term graded profile of delta top. Negative values represent available accommodation with positive values representing negative accommodation.

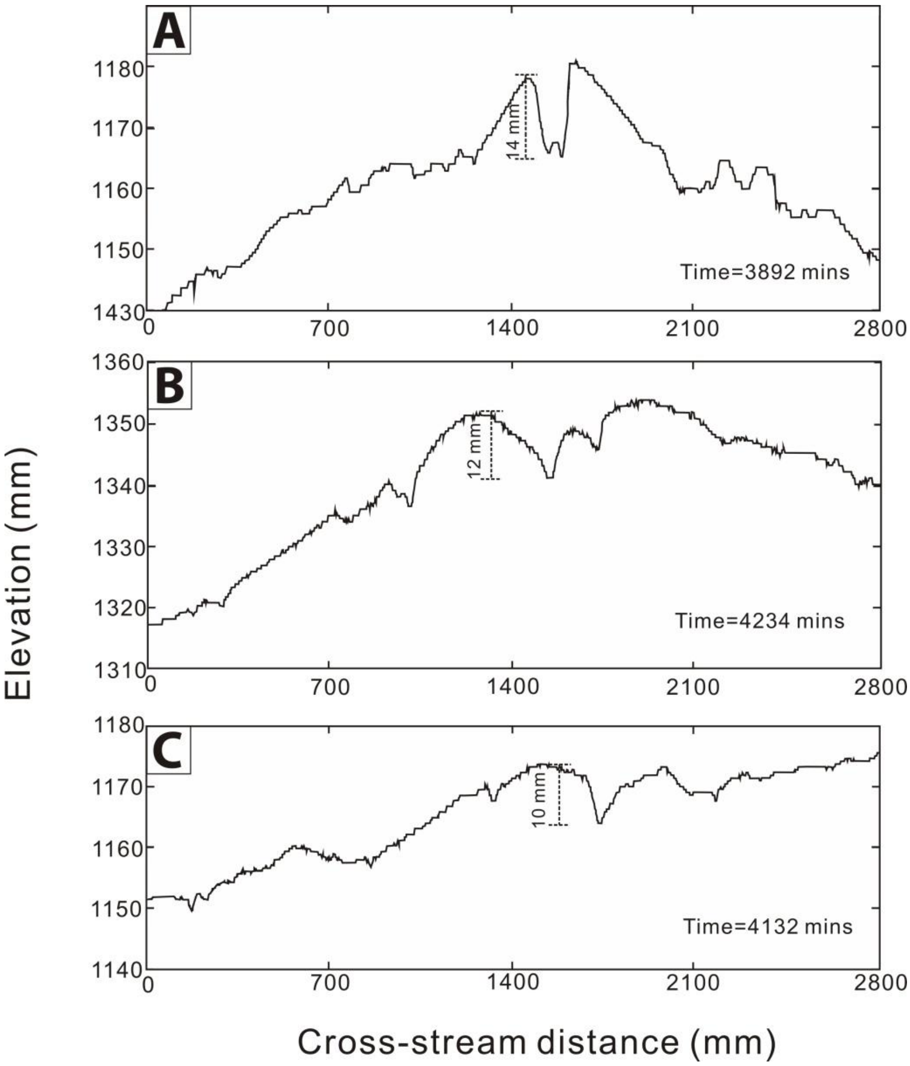

Figure 8: Elevation cross sections showing deepest channels observed in the TDB 10-1 experiment at the (A) proximal, (B) medial, and (C) distal measurement transects.

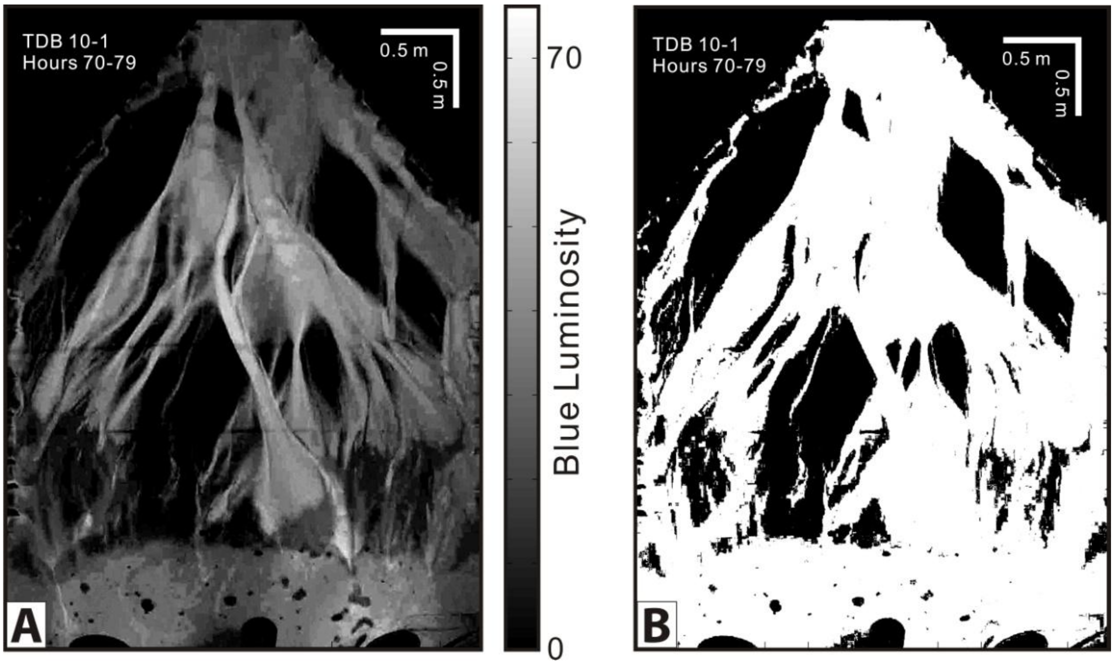

Figure 9: Maps defining flow field of the TDB 10-1 experiment at 76 hrs of run time. A) Map defining intensity of blue luminosity of active surface (Figure 6). Intensity values range from 0 (no blue intensity) to 75 (pure blue intensity). B) Binary image showing wet (white) regions and dry (black) regions. Wet and dry regions were identified through threshold blue luminosity analysis outlined in Section 5. The threshold luminosity used in our analysis is 10.

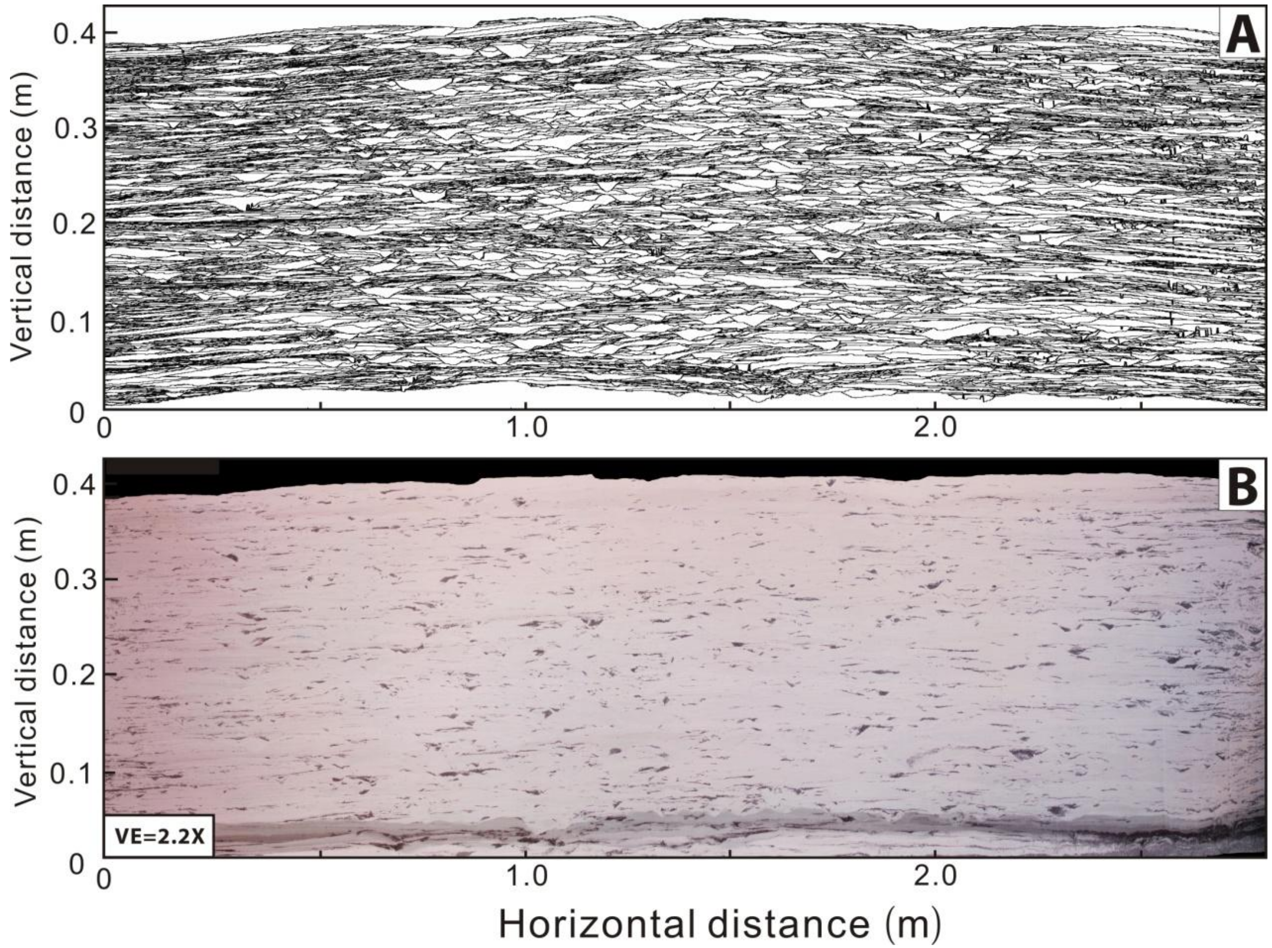

Figure 10: Experimental stratigraphy of the TDB 10-1 proximal measurement transect. A) Synthetic stratigraphy generated through stacked delta-top profiles with topography clipped to account for sediment removed during erosional events. B) Image of preserved physical stratigraphy sliced in the cross-stream direction.

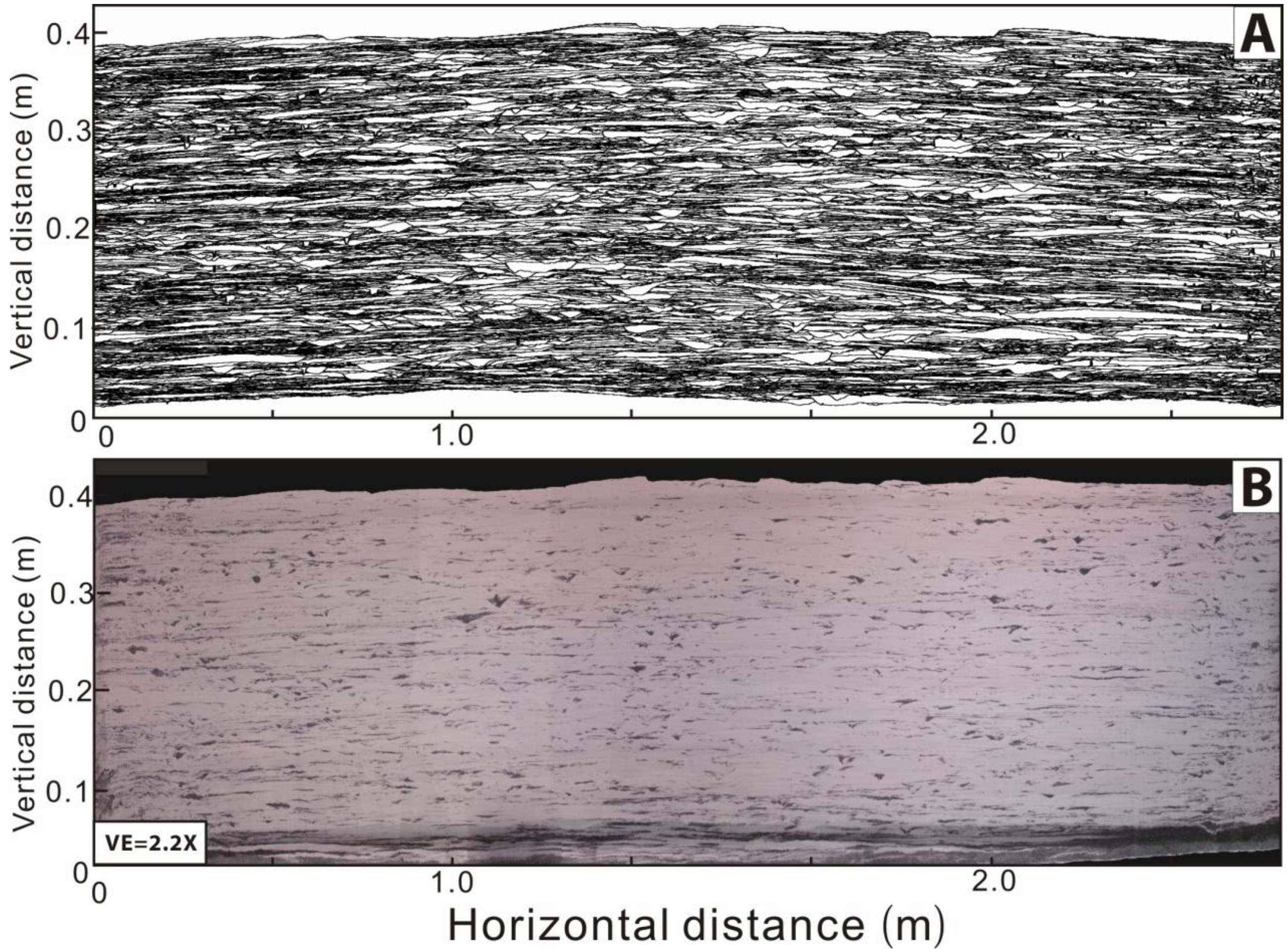

Figure 11: Experimental stratigraphy of the TDB 10-1 medial measurement transect. A) Synthetic stratigraphy generated through stacked delta-top profiles with topography clipped to account for sediment removed during erosional events. B) Image of preserved physical stratigraphy sliced in the cross-stream direction.

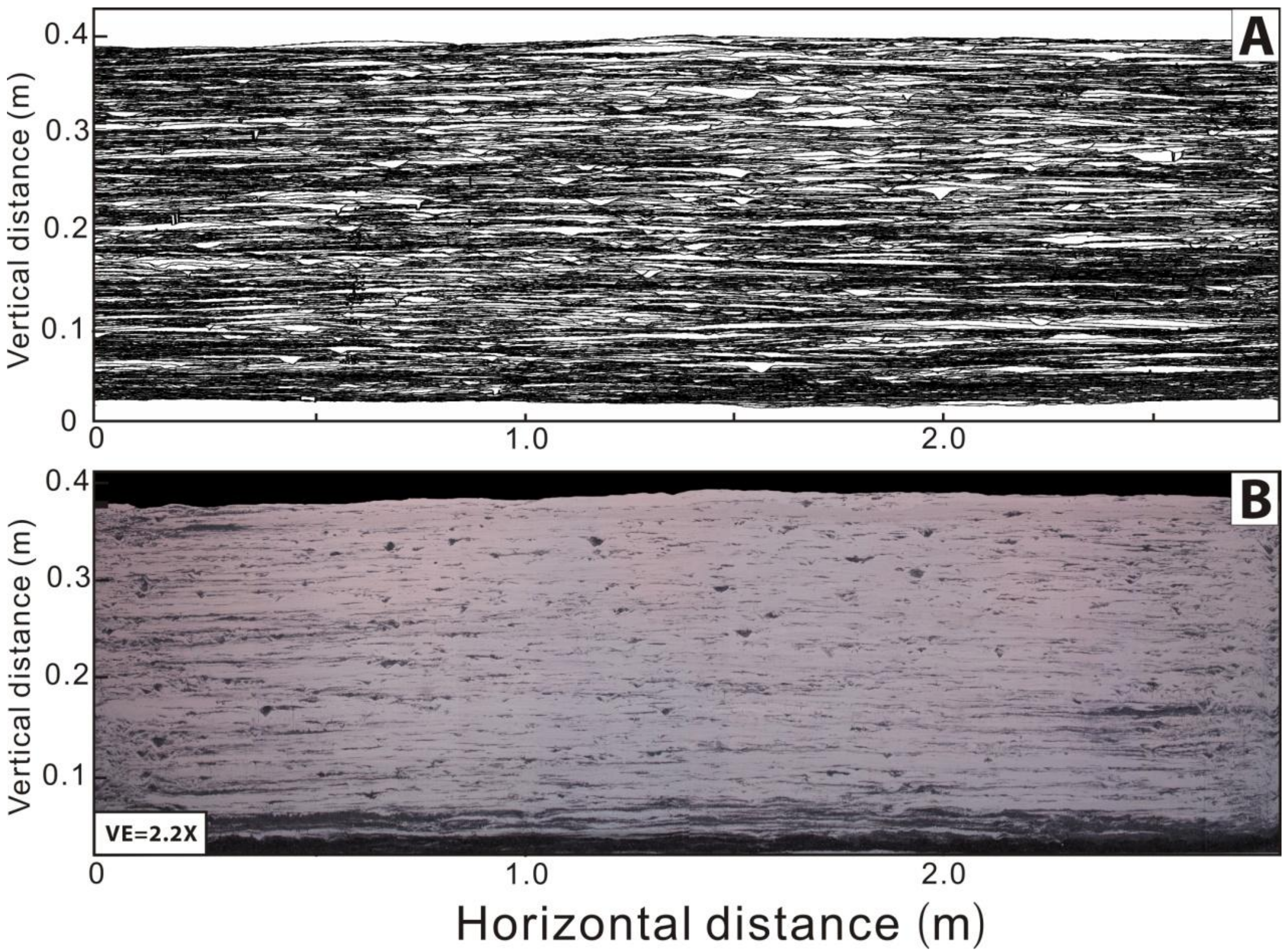

Figure 12: Experimental stratigraphy of the TDB 10-1 distal measurement transect. A) Synthetic stratigraphy generated through stacked delta-top profiles with topography clipped to account for sediment removed during erosional events. B) Image of preserved physical stratigraphy sliced in the cross-stream direction.

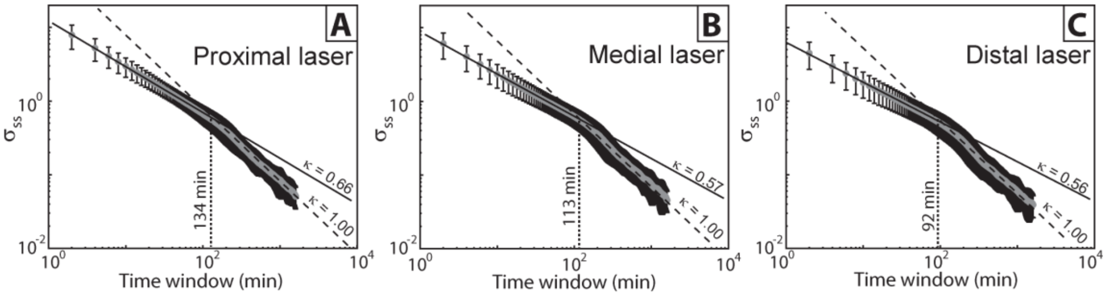

Figure 13: σ_{ss} decays in the time domain as a power law for the three laser transects in TDB 10-1 with κ < 0.7 beneath T_C and κ = 1.0 above T_C. Trend lines and associated κ values represent best fit linear regression to log-log data with data in each plot separated into two segments at T_C. Error bars represent geometric standard deviation.

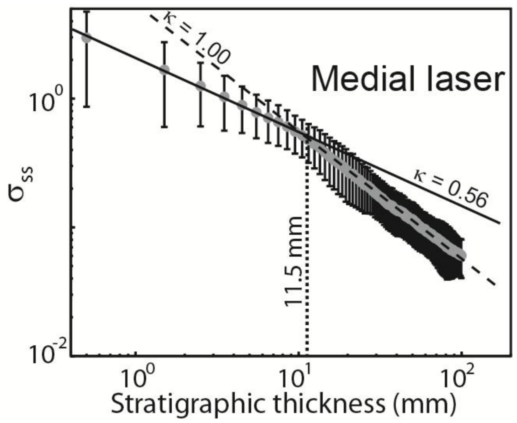

Figure 14: σ_{ss} decays in the space domain as a power law with near identical values of κ as found in the time domain. Error bars represent geometric standard deviation.

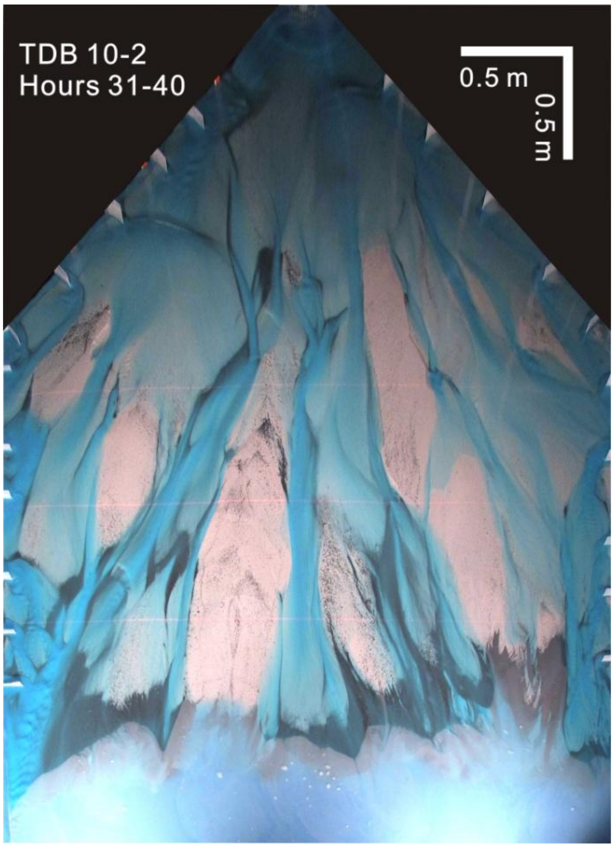

Figure 15: Overhead photograph taken at 35 hours into the aggradational phase of TDB 10-2 experiment. Flow is dyed blue to aid visualization. System is approximately 3.1 m in length from source to shoreline.

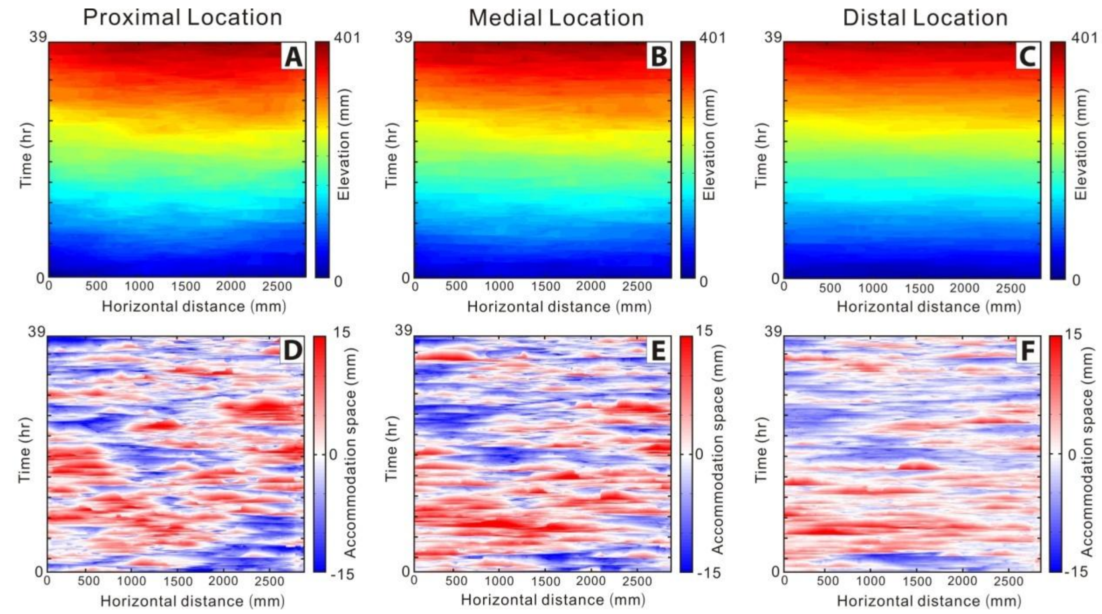

Figure 16: Data defining evolution of topography and surface dynamics for the TDB 10-2 experiment at the three measurement transects. A-C) Time-space plots of sequential delta-top profiles for the three measurement transects shown every 2 min for the course of the 39 hr experiment. D-F) Accommodation-space plots calculated from time-space data. Accommodation represents distance below long term graded profile of delta top. Negative values represent available accommodation with positive values represent negative accommodation.

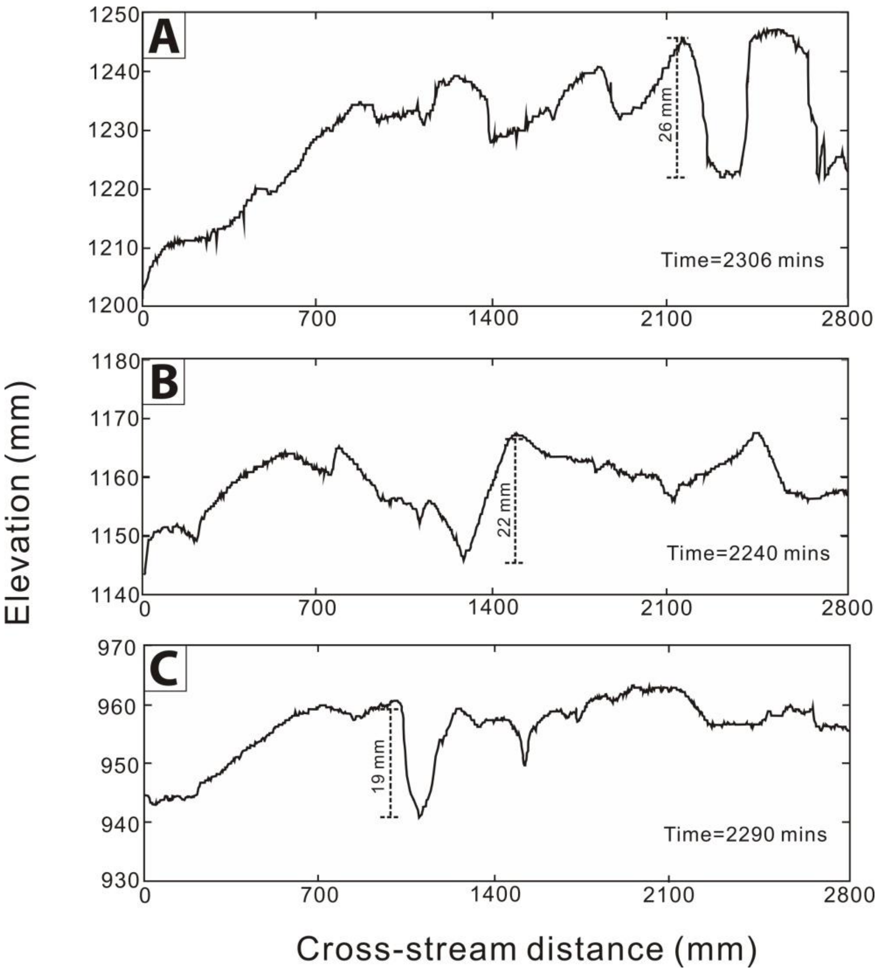

Figure 17: Elevation cross sections showing deepest channels observed in the TDB 10-2 experiment at the (A) proximal, (B) medial, and (C) distal measurement transects.

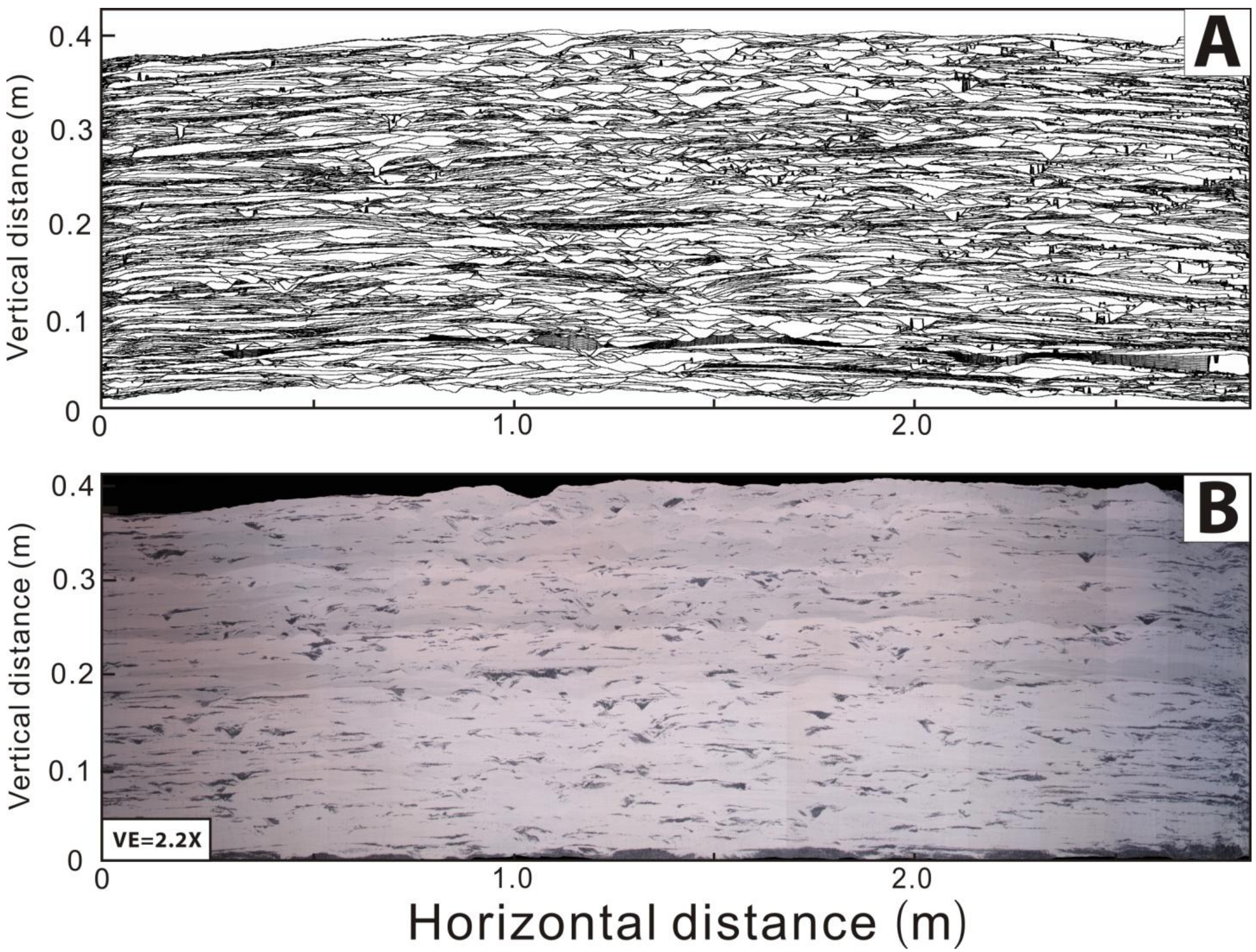

Figure 18: Experimental stratigraphy of the TDB 10-2 proximal measurement transect. A) Synthetic stratigraphy generated through stacked delta-top profiles with topography clipped to account for sediment removed during erosional events. B) Image of preserved physical stratigraphy sliced in the cross-stream direction.

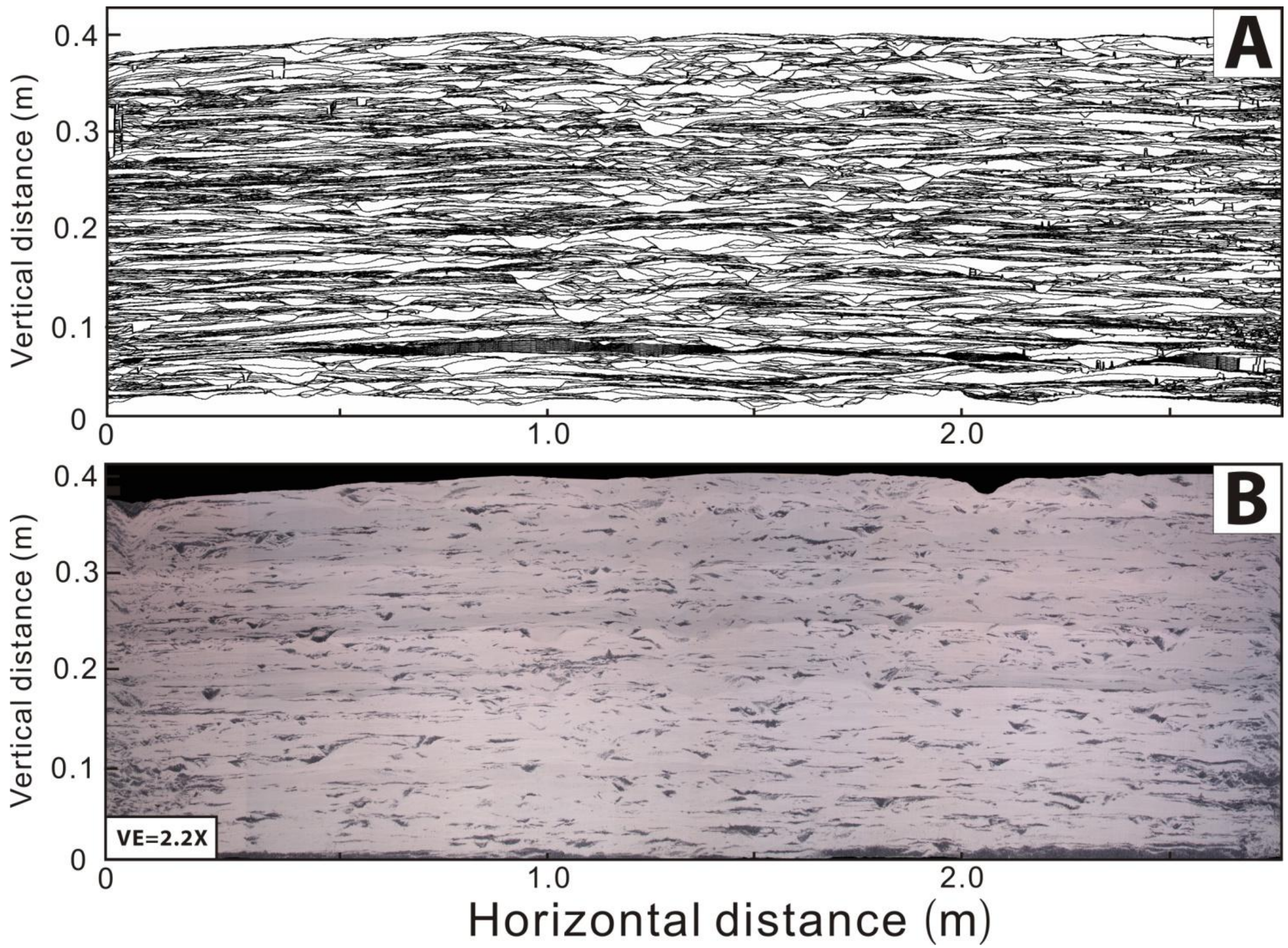

Figure 19: Experimental stratigraphy of the TDB 10-2 medial measurement transect. A) Synthetic stratigraphy generated through stacked delta-top profiles with topography clipped to account for sediment removed during erosional events. B) Image of preserved physical stratigraphy sliced in the cross-stream direction.

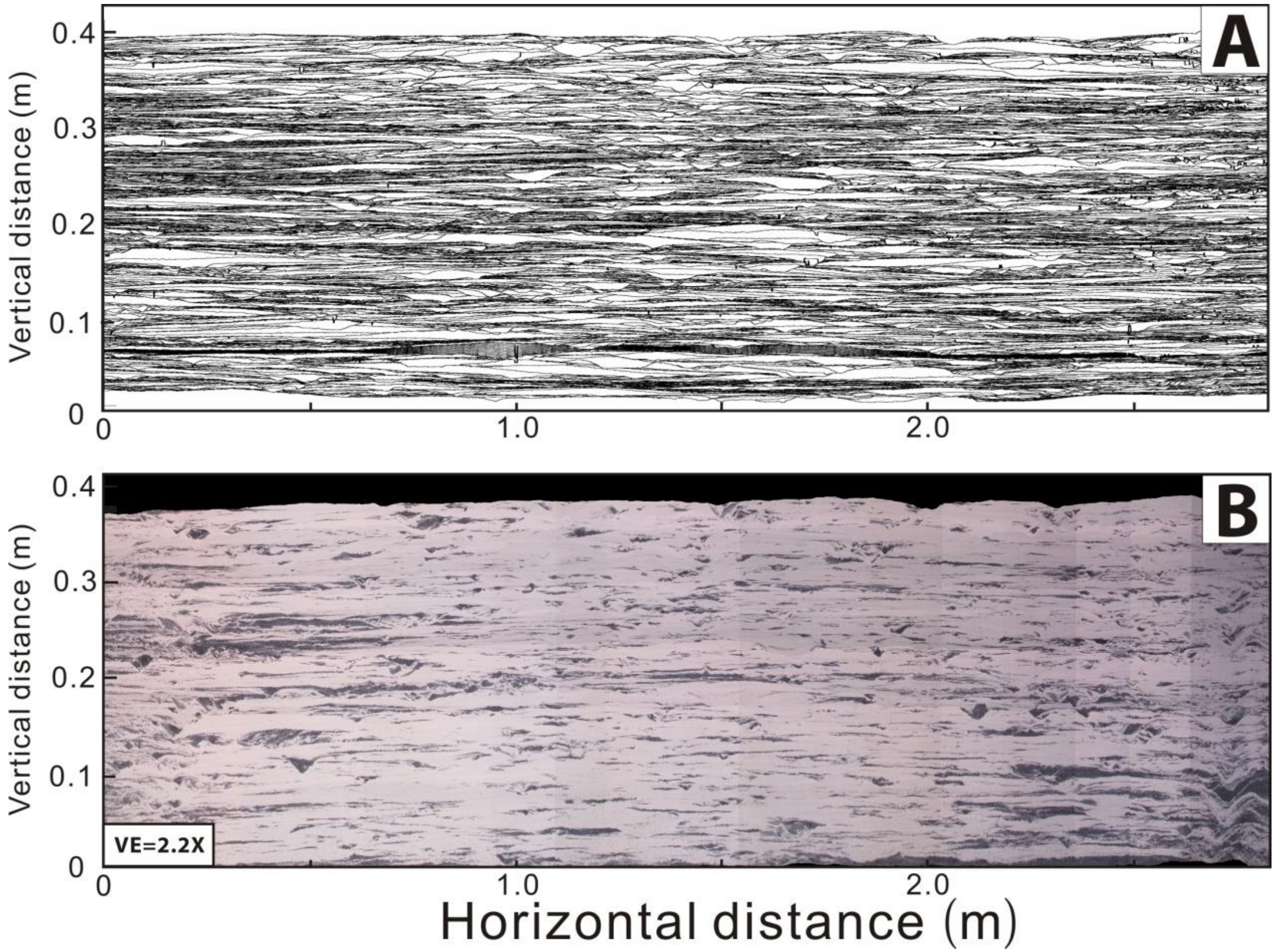

Figure 20: Experimental stratigraphy of the TDB 10-2 distal measurement transect. A) Synthetic stratigraphy generated through stacked delta-top profiles with topography clipped to account for sediment removed during erosional events. B) Image of preserved physical stratigraphy sliced in the cross-stream direction.

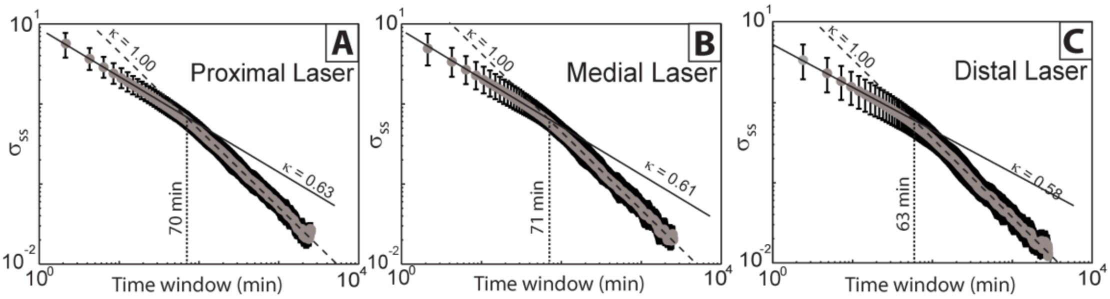

Figure 21: σ_{ss} decays in the time domain as a power law for the three laser transects in TDB 10-2 with $\kappa < 0.7$ beneath T_C and $\kappa = 1.0$ above T_C. Trend lines and associated κ values represent best fit linear regression to log-log data with data in each plot separated into two segments at T_C. Error bars represent geometric standard deviation.

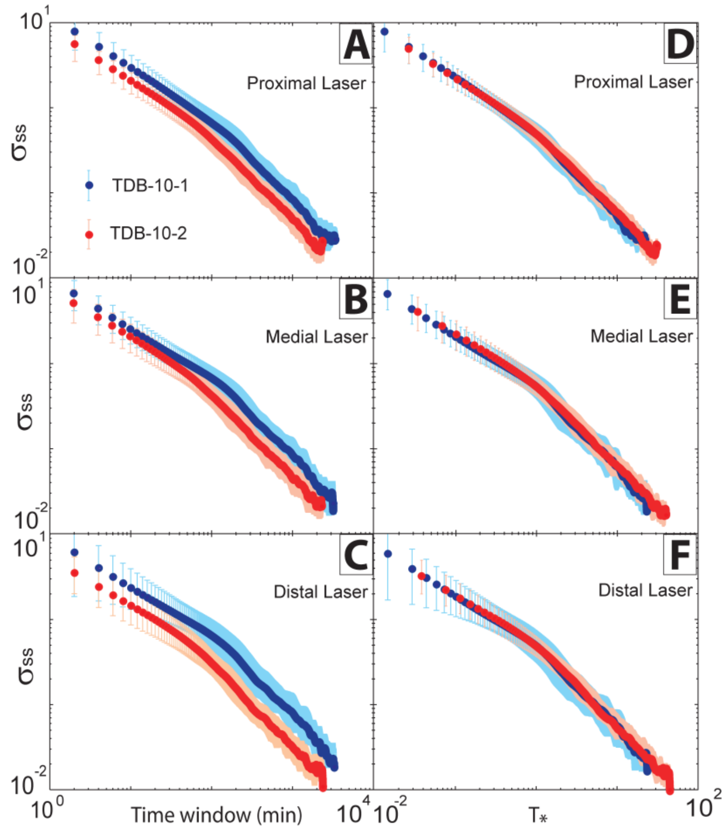

Figure 22: Comparison of the decay of σ_{ss} in the time domain for the TDB 10-1 and TDB 10-2 experiments. Comparison is made in both dimensional (A-C) and non-dimensional (D-F) time space. In the non-dimensional time space, the decay of σ_{ss} shows a similar pattern in the two experiments, which indicates on each transect the κ values are near identical and otherwise compensation time scales are distinct to some extent. Error bars represent geometric standard deviation.

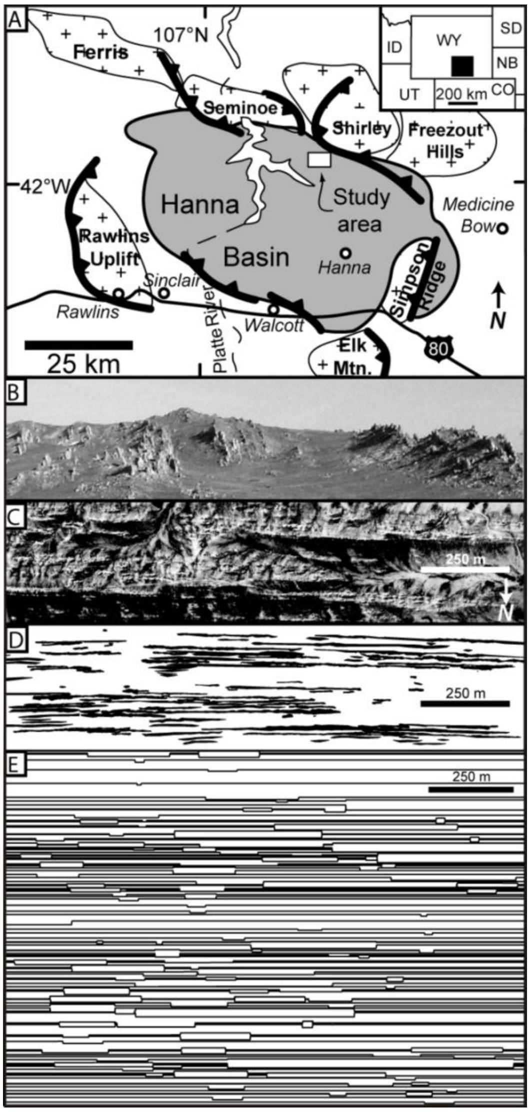

Figure 23: A) Location map of the study area (after Eberle and Lillegraven, 1998) showing the greater Hanna Basin (gray) and major structures and uplifts (crosses). B) Field photo of the Ferris Fm. Strata dip 80° (to the right) and sandstone channel deposits stand out in relief against more heavily weathered overbank mudstones. C) Air photo of study area showing across-section of the Ferris Fm. exposed across the land surface. Average paleoflow direction is into the photo. Channel-belt sandstones are visible as white elongate bodies. D) Channel sand bodies (black) from C mapped with differential GPS. Centroids of these bodies were used for clustering analysis. E) Pseudo horizons used for compensation analysis follow the mean base of each sand body and extend laterally away from the sand body into floodplain deposits. Vertical exaggeration is ~2.5.

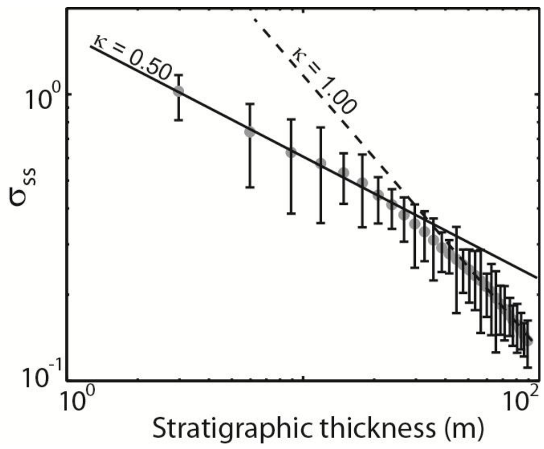

Figure 24: Decay of σ_{ss} as a function of stratigraphic thickness for the Ferris Formation showing random filling at small (< 10 m) of thickness and compensational filling for large (> 40 m) stratigraphic thickness. Error bars represent geometric standard deviation.

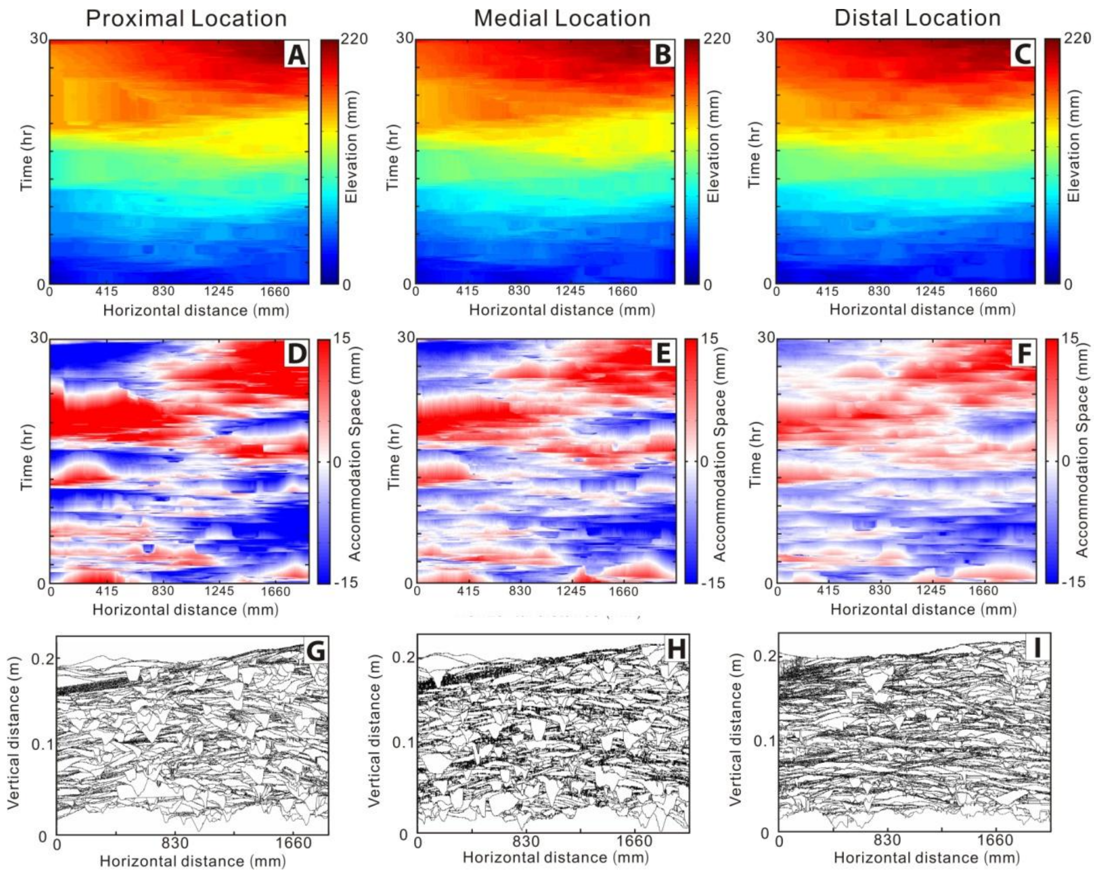

Figure 25: Data defining evolution of topography, surface dynamics, and resulting stratigraphy for the DB-03 experiment at the three measurement transects. A-C) Time-space plots of sequential delta-top profiles for the three measurement transects shown every 2 min for the course of the 30 hr experiment. D-F) Accommodation-space plots calculated from time-space data. Accommodation represents distance below long term graded profile of delta top. Negative values represent available accommodation with positive values represent negative accommodation. G-I) Synthetic stratigraphy generated through stacked delta-top profiles with topography clipped to account for sediment removed during erosional events.

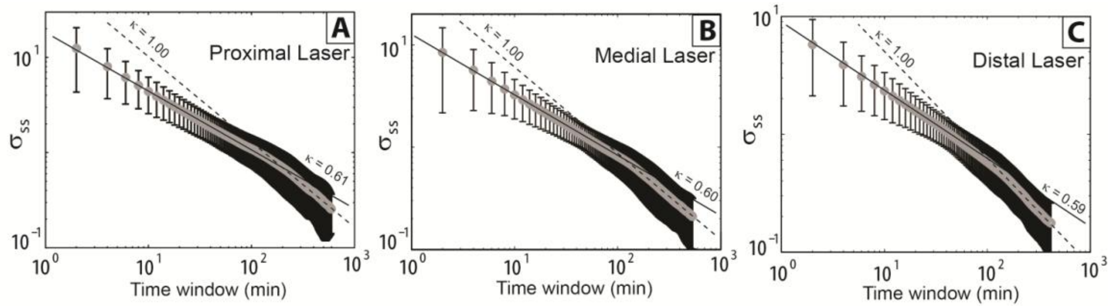

Figure 26: σ_{ss} decays in the time domain as a power law for the three laser transects in DB-03 with $\kappa < 0.7$ beneath T_C and $\kappa = 1.0$ above T_C. Trend lines and associated κ values represent best fit linear regression to log-log data with data in each plot separated into two segments at T_C. Error bars represent geometric standard deviation.

Figure 27: Photograph taken approximately 15.0 hr into the DB-03 experiment. System is approximately 2.5 m in length from source (back center) to shoreline. Topographic measurements were taken along three laser sheet lines located 1.5 m, 1.75 m and 2.0 m from sediment source.

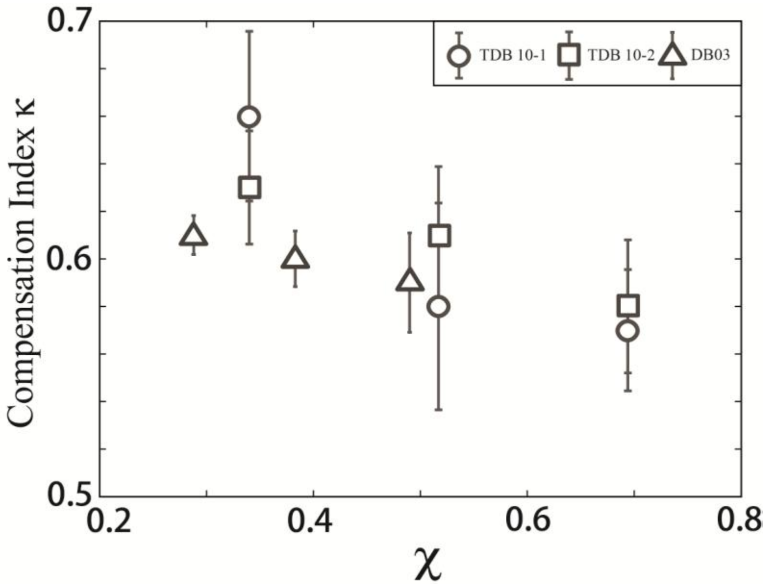

Figure 28: Comparison of the decay of κ with increasing χ in TDB 10-1, TDB 10-2 and DB-03 experiments. Utilizing χ allows for comparison of stratigraphic organization in experiments with different deposit In all three experiments we note a decrease in κ with increasing χ. Error bars represent geometric standard deviation of κ estimates performed over time windows initiating at the temporal resolution of the data and terminating between 1/2 T_c and T_c.

TABLES

Experiment	Q_w (L/sec)	Q_s (L/sec)	Ratio Q_w/Q_s	Average aggradation rate (mm/hr)
TDB 10-1	0.451	0.011	41	5
TDB 10-2	0.902	0.022	41	10
Q_w, total volumetric water discharge; Q_s, total volumetric sediment discharge				

Table 1: Input conditions of TDB 10-1 and TDB 10-2.

Location	wetted fraction		Channel depth (in mm)		T_C (in min)		κ	
	TDB 10-1	TDB 10-2	TDB 10-1	TDB 10-2	TDB 10-1	TDB 10-2	TDB 10-1	TDB 10-2
Proximal	0.5385	0.6267	11.2	11.7	134	70	0.656	0.628
medial	0.5875	0.6277	9.4	11.8	113	71	0.577	0.608
distal	0.597	0.7231	7.7	8.8	92	53	0.568	0.58

Table 2: Comparison of experimental parameters in two experiments.

APPENDIX: Code for 2-D object-based stacking model

```
bw=50; % basin width
wh=1000;%model window height
st=2; % deposit thickness
at=60;% avulsion time scale
data=[];
topo=zeros(1,bw);
thr=14; % roughness length
NumberOfPlots=10;
ColorSet=varycolor(NumberOfPlots);
m=1;
for unit=1:100
    unit
    r=unit-1;
    n=round(rand(1,1)*10);
    lastn=n;
    if n==0
      n=round(rand(1,1)*10);
    end
    if n==lastn
      n=round(rand(1,1)*10);
    end
    if m==1
        plot(topo(1,:),'color',ColorSet(n,:));
        axis([1 bw 0 wh]);
        legend off
        set(gcf, 'Colormap', ColorSet);
        colorbar
        hold on
        ran=round(rand(1,1)*bw);
        if ran>=2 & ran<bw
            topo(1,ran)=st;
            topo(1,ran-1)=1;
            topo(1,ran+1)=1;
            plot(topo(1,:),'color',ColorSet(n,:));
            axis([1 bw 0 wh]);
            hold on
        end
        if ran==0
              ran=1;
        end
        if ran==1
```

```
            topo(1,ran)=st;
            topo(1,bw)=1;
            topo(1,ran+1)=1;
            plot(topo(1,:),'color',ColorSet(n,:));
            axis([1 bw 0 wh]);
            hold on
        end
        if ran==bw
            topo(1,bw)=st;
            topo(1,bw-1)=1;
            topo(1,1)=1;
            plot(topo(1,:),'color',ColorSet(n,:));
            axis([1 bw 0 wh]);
            hold on
        end
        data(1+r*at,:)=topo(1,:);
        m=m+1;
    end
    if unit > 1
         for b=1:bw
             if topo(1,b)==min(topo(1,1:bw))
                 ran=b;
             end
         end
        if ran>=2 & ran<bw
        topo(1,ran)=topo(1,ran)+st;
        topo(1,ran-1)=topo(1,ran-1)+1;
        topo(1,ran+1)=topo(1,ran+1)+1;
        plot(topo(1,:),'color',ColorSet(n,:));
        axis([1 bw 0 wh]);
        hold on
        end
        if ran==1
            topo(1,ran)=topo(1,ran)+st;
            topo(1,bw)=topo(1,bw)+1;
            topo(1,ran+1)=topo(1,ran+1)+1;
            plot(topo(1,:),'color',ColorSet(n,:));
            axis([1 bw 0 wh]);
            hold on
        end
        if ran==bw
            topo(1,bw)=topo(1,bw)+st;
            topo(1,bw-1)=topo(1,bw-1)+1;
            topo(1,1)=topo(1,1)+1;
```

```
                plot(topo(1,:),'color',ColorSet(n,:));
                axis([1 bw 0 wh]);
                hold on
            end
        data(1+r*at,:)=topo(1,:);
        end
for i=2:at
        a=round(rand(1,1));
        ave=mean(topo(1,:));
        peak=ave+thr;
        if ran~=bw
            if topo(1,ran+1)>=peak
                a=0;
            end
        else
                if topo(1,1)>=peak
                        a=0;
                end
        end

        if ran~=1
              if topo(1,ran-1)>=peak
                a=1;
              end
        else
                if topo(1,bw)>=peak
                a=1;
                end
        end
if a==1
        if ran==bw
                  topo(1,1)=topo(1,1)+st;
                  topo(1,2)=topo(1,2)+1;
                  topo(1,bw)=topo(1,bw)+1;
                  axis([1 bw 0 wh]);
                  plot(topo(1,:),'color',ColorSet(n,:));
                  ran=1;
                  hold on
elseif ran~=bw
                topo(1,ran+1)=topo(1,ran+1)+st;
                plus=ran+2;
                if plus<=bw
                        topo(1,ran+2)=topo(1,ran+2)+1;
                end
```

```
            if plus>bw
                topo(1,1)=topo(1,1)+1;
            end
            topo(1,ran)=topo(1,ran)+1;
            axis([1 bw 0 wh]);
            plot(topo(1,:),'color',ColorSet(n,:));
            ran=ran+1;
            hold on
        end
    end
        if a==0
            if ran==1
                topo(1,bw)=topo(1,bw)+st;
                topo(1,1)=topo(1,1)+1;
                topo(1,bw-1)=topo(1,bw-1)+1;
                axis([1 bw 0 wh]);
                plot(topo(1,:),'color',ColorSet(n,:));

                ran=bw;
                hold on
          elseif ran~=1
            topo(1,ran-1)=topo(1,ran-1)+st;
            diff=ran-2;
            if diff>=1
            topo(1,ran-2)=topo(1,ran-2)+1;
            end
            if diff<1
              topo(1,bw)=topo(1,bw)+1;
            end
            topo(1,ran)=topo(1,ran)+1;
            axis([1 bw 0 wh]);
            plot(topo(1,:),'color',ColorSet(n,:));
            ran=ran-1;
            hold on
         end
      end
        pause(0.05);
        data(i+r*at,:)=topo(1,:);

      end
    end
```

REFERENCES

Ager, D.V., 1973, The Nature of the Stratugraphic Record: New York, Wiley, 114 p.

Allen, J.R.L., 1965, A review of the origin and characteristics of recent alluvial sediments, Sedimentology, v.5, p. 89-101.

Aslan, A., Autin, W.J., and Blum, M.D., 2005, Causes of river avulsion: Insights from the Late Holocene avulusion history of the Mississippi River, U.S.A.: Journal of Sedimentary Research, v. 75, p. 650-664.

Beerbower, J.R., 1964, Cyclothems and cyclic depositional mechanisms in alluvial plain sedimentation, Merriam, D.F. (Ed.), Symposium on cyclic sedimentation. Bull. Kansas Geol. Survey, v. 169.2.1.6, p. 31-42.

Blum, M.D., and Tornqvist, T.E., 2000, Fluvial responses to climate and sea-level change: a review and look forward, Sedimentology, v. 47, p. 2-48.

Clarke L., Quine, T., and Nicholas, A., 2010, An experiemntal investigation of autogenic behaviour during alluvial fan evolution: Geomorphology, v. 115, p. 278-285.

Coleman, J.M., 1988, Dynamic changes and processes in the Mississippi River Delta: Geological Society of America Bulletin, v. 100, p. 999-1015.

Covault, J.A., Romans, B.W., Fildani, A., McGann, M., and Graham, S.A., 2010, Rapid Climatic Signal Propagation from Source to Sink in a Southern California Sediment-Routing System: Journal of Geology, v. 118, p. 247-259.

Csato, I., Kendal, C. G.St.C., 2002, Modeling of stratigraphic architectural patterns in extensional settings-towards a conceptual model: Computers & Geosciences, v. 28, p. 351–356.

Deptuck, M.E., Piper, D.J.W., Savoye, B., and Gervais, A., 2008, Dimensions and architecture of late Pleistocene submarine lobes off the northern margin of East Corsica: Sedimentology, v. 55, p. 869-U34.

Deptuck, M.E., Sylvester, Z., Pirmez, C. and O'Byrne, C., 2007, Migration–aggradation history and 3-D seismic geomorphology of submarine channels in the Pleistocene Benin-major Canyon, western Niger Delta slope: Marine and Petroleum Geology, v. 24, p. 406-433.

Dorsey, R.J., Umhoefer, P.J. and Falk, P.D., 1997, Earthquake clustering inferred from Pliocene Gilbert-type fan deltas in the Loreto basin, Baja California Sur, Mexico: Geology, v. 25, n. 8, p. 679-682.

Eberle, J.J., and Lillegraven, J.A., 1998, A new important record of earliest Cenozoic mammalian history: Geologic setting, Multituberculata, and Peradectia: Rocky Mountain Geology, v. 33, p. 3-47.

Edmonds, D.A., and Slingerland, R.L., 2010, Significant effect of sediment cohesion on delta morphology: Nature Geoscience, v. 3, p. 105-109.

Euzen T., Joseph P., Du Fornel E., Lesur S., Granjeon D. and Guillocheau F., 2004, Three-dimensional stratigraphic modelling of the Grès d’Annot system, Eocene-Oligocene, SE France: Geological Society, London, Special Publications, v. 221, p.161-180.

Gagliano, S.M., 2005, Effects of earthquakes, fault movements, and subsidence on the south Louisiana landscape: The Louisiana Civil Engineer Journal, v. 13, n. 2, p. 19-22.

Ganti, V., Straub, K.M., Foufoula-Georgiou, E., and Paola, C., in press, Space-time dynamics of depositional systems: Experimental evidence and theoretical modeling of heavy-tailed statistics: Journal of Geophysical Research, p. 16.

Galloway, W.E., Ganey-Curry, P.E., Li, X., and Buffler, R.T., 2000, Cenozoic depositional history of the Gulf of Mexico basin: AAPG Bulletin, v. 84, p. 1743-1774.

Gupta, S., Cowie, P.A., Dawers, N.H. and Underhill, J.R., 1998, A mechanism to explain rift-basin subsidence and stratigraphic patterns through fault-array evolution: Geology, v. 26, n. 7, p. 595-598.

Hajek, E.A., 2009, Characterizing and interpreting channel-body clustering in the Ferris Formation, Hanna Basin, Wyoming [Ph.D. thesis], University of Wyoming.

Hajek, E.A., Heller, P.L., and Sheets, B.A., 2010, Significance of channel-belt clustering in alluvial basins: Geology, v. 38, p. 535-538.

Hardy, S., Gawthorpe, R.L., 1998, Effects of variations in fault slip rate on sequence stratigraphy in fan deltas: insights from numerical modeling: Geology, v. 26, p. 911–914.

Heller, P.L., Paola, C., Hwang, I., John, B., and Steel, R., 2001, Geomorphology and sequence stratigraphy due to slow and rapid base-level changes in an experimental subsiding basin (XES 96-1): AAPG Bulletin, v. 85, p. 817-838.

Hofmann, M.H., Wroblewski, A. and Boyd, R., 2011, Mechanisms controlling the clustering of fluvial channels and the compensational stacking of cluster belts: Journal of Sedimentary Research, v. 81, p. 670-685.

Hooke, R.L., 1968, Model geology:prototype and laboratory streams: discussion, Geological Society of America Bulletin v. 79, p. 391-394.

Hoyal, D.C.J.D., and Sheets, B.A., 2009, Morphodynamic evolution of experimental cohesive deltas: Journal of Geophysical Research-Earth Surface, v. 114, F02009.

Jerolmack, D.J., and Paola, C., 2007, Complexity in a cellular model of river avulsion: Geomorphology, v. 91, p. 259-270.

Jerolmack, D.J., and Paola, 2010, Shredding of environmental signals by sediment transport: Geophysical Research Letters, v. 37, p. L19401.

Kendall, C.G.St.C., Strobel, J., Cannon, R.L., Bezdek, J., Biswas, G., 1991, The simulation of the sedimentary fill of basins: Journal of Geophysical Research, v. 96, p. 6911–6929.

Kim, W., Paola, C., Swenson, J.B., and Voller, V.R., 2006, Shoreline response to autogenic processes of sediment storage and release in the fluvial system: Journal of Geophysical Research-Earth Surface, v. 111, p. -.

Kim, W., and Paola, C., 2007, Long-period cyclic sedimentation with constant tectonic forcing in an experimental relay ramp: Geology, v. 35, p. 331-334.

Kim, W., and Jerolmack, D.J., 2008, The pulse of calm fan deltas: The Journal of Geology, v. 116, p. 315-330.

Kleinhans, M.G., 2005, Autogenic cyclicity of foreset sorting in experimental Gilbert-type deltas: Sedimentary Geology, v. 181, p. 215 – 22.

Kubo, Y., Syvitski, J.P.M., Hutton, E.W.H., and Paola, C., 2005, Advance and application of the stratigraphic simulation model 2D-SedFlux: From tank experiment to geological scale simulation: Sedimentary Geology, v. 178, p. 187-195.

Kulp, M., Howell, P., Adiau, S., Penland, S., Kindinger, J., and Williams, S.J., 2002, Latest Quaternary stratigraphic framework of the Mississippi delta region: Gulf Coast Association of Geological Societies Transactions, v. 52, p. 572-582.

Lyons, W.J., 2004, Quantifying channelized submarine depositional systems from bed to basin scale [Ph.D. thesis]: Cambridge, Massachusetts Institute of Technology.

Mack, G. H. and Rasmussen, K.A, 1984; Alluvial-fan sedimentation of the Cutler Formation (Permo-Pennsylvanian) near Gateway, Colorado: *GSA Bulletin*, v. 95; no. 1; p. 109-116.

Marco, S., Mordechai, S., and Agnon, A., 1996, Longterm earthquake clustering: A 50,000-year paleoseismic record in the Dead Sea graben: Journal of Geophysical Research, v. 101, p. 6179–6191.

Martin, J., 2007, Quantitative sequence stratigraphy [unpublished Ph.D. thesis]: University of Minnesota, Minneapolis, Minnesota, 193 p.

Martin, J., Sheets, B. C., Paola, C. and Hoyal, D., 2009a, Influence of steady base-level rise on channel mobility, shoreline migration, and scaling properties of a cohesive experimental delta: Journal of Geophysical Research, v. 114/F3, p. Citation F03017, doi:10.1029/2008JF001142.

Martin, J., Paola, C., Abreu, V., Neal, J., and Sheets, B., 2009b, Sequence stratigraphy of experimental strata under known conditions of differential subsidence and variable base level: AAPG Bulletin, v. 93, p. 503-533.

Metivier, F., Lajeunesse, E., and Cacas, M.C., 2005, Submarine canyons in the bathtub: Journal of Sedimentary Research, v. 75, p. 6-11.

Miall, A.D., 1996, The Geology of Fluvial Deposits: Sedimentary Facies, Basin Analysis, and Petroleum Geology: New York, Springer, 582 p.

Mohrig, D., Heller, P.L., Paola, C., and Lyons, W.J., 2000, Interpreting avulsion process from ancient alluvial sequences: Guadalope-Matarranya (northern Spain) and Wasatch Formation (western Colorado): GSA Bulletin, v. 112, p. 1787-1803.

Muto, T., 2001, Shoreline autoretreat substantiated in flume experiments: Journal of

Sedimentary Research, v. 71, p. 246-254.

Muto, T., and Swenson, J.B., 2005, Large-scale fluvial grade as a non-equilibrium state in linked depositional systems: Theory and experiment, Journal of Geophysical Research-Earth Surface, v. 110, p. F03002.

Muto, T. and Steel, R.J., 2004, Autogenic response of fluvial deltas to steady sea-level fall: implications from flume-tank experiments: Geology, v. 32, p. 401-404.

Muto, T., Steel, R.J., and Swensn, J.B., 2007, Autostratigraphy: a framework norm for genetic stratigraphy, Journal of Sedimentary Research, v. 77, p. 2-12.

Mutti, E., and Sonnino, M., 1981, Compensational cycles: A diagnostic feature of turbidite sandstone lobes (abstract), International Association of Sedimentologist, Second European Regional Meeting, p. 120-123.

Olariu, C., and Bhattacharya, J.P., 2006, Terminal distributary channels and delta front architecture of river-dominated delta systems: Journal of Sedimentary Research, v. 76, p. 212-233.

Paola, C., 2000, Quantitative models of sedimentary basin filling: Sedimentology, v. 47, p. 121-178.

Paola, C., and Borgman, L., 1991, Reconstructing random topography from preserved stratification: Sedimentology, v. 38, p. 553-565.

Paola, C., Heller, P.L., and Angevine, C.L., 1992, The large-scale dynamics of grain-size variation in alluvial basins, 1: Theory: Basin Research, v. 4, p. 73-90.

Paola, C., Straub, K.M., Mohrig, M., and Reinhardt, L., 2009, The "unreasonable effectiveness" of stratigraphic and geomorphic experiemnts: Earth-Science Reviews, v. 97, p. 1-43.

Parker, G., Paola, C., Whipple, K. X., and Mohrig, D., 1998, Fluvial Fans: Theory: Jour. Hydr. Eng., v. 124, n. 10, p. 1-11.

Peper, T. and Cloetingh, S., 1995, Autocyclic perturbations of orbitally forced signals in the sedimentary record: Geology, v. 23; no. 10; p. 937-940;

Perlmutter, M.A., Radovich, B.J., Matthews, M.D., and Kendall, C.G.S.C., 1998, The impact of high-frequency sedimentation cycles on stratigraphic interpretation, in Grandstein, F.M., Sandvik, K.O., and Milton, N.J., eds., Sequence stratigraphy - Concepts and Applications. Special Publication of the

Norwegian Petroleum Society, p. 141-170.

Pirmez, C., Beaubouef, R.T., Friedmann, S.J., and Mohrig, D., 2000, Equilibrium profile and baselevel in submarine channels: examples from Late Pleistocene systems and implications for the architecture of deepwater reservoirs, GCSEPM Foundation 20th Annual Research Conference, Deep-Water Reservoirs of the World, p. 782-805.

Pitman, W.C., 1978, Relationship between eustacy and stratigrahic sequences on passive margins: GSA Bulletin, v. 89, p. 1389-1403.

Prosser, S., 1993, Rift-related linked depositional systems and their seismic expression, in Williams, G. D., and Dobb, A., eds., Tectonics and seismic sequence stratigraphy: Geological Society [London] Special Publication 71, p. 117–144.

Pyles, D.R., 2007, Architectural elements in a ponded submarine fan, Carboniferous Ross Sandstone, western Ireland, in Nilsen, T.H., Shew, R.D., Steffens, G.S., and Studlick, J.R.J., eds., Atlas of deep-water outcrops: AAPG Studies in Geology 56, CD-ROM, p. 19.

Reitz, M.D., Jerolmack, D.J. and Swenson, J.B., 2010, Flooding and flow path selection on alluvial fans and deltas: Geophysical Research letters, v. 37, L06401.

Samuel, A., Kneller, B., Raslan, S., Sharp, A. and Parsons, C., 2003, Prolific Deep Marine Slope Channels of the Nile Delta, Egypt: AAPG Bulletin, v. 87, p. 541–560.

Schwab, A.M., Cronin, B.T. and Ferreira, H., 2007, Seismic expression of channel outcrops: Offset stacked versus amalgamated channel systems: Marine and Petroleum Geology, v. 24, p. 504-514.

Sheets, B., Hickson, T.A., and Paola, C., 2002, Assembling the stratigraphic record: depositional patterns and time scales in an experimental alluvial basin: Basin Research, v. 14, p. 287-301.

Sheets, B.A., Paola, C., and Kelberer, J.M., 2007, Creation and preservation of channel-form sand bodies in an experimental alluvial system, *in* Nichols, G., Williams, E., and Paola, C., eds., Sedimentary Processes, Environments and Basins: Oxford, U.K., Blackwell Publishing, p. 555-567.

Slingerland, R.L., 1990, Predictability and chaos in quantitative dynamic stratigraphy, *in* Cross, T.A., ed., Quantitative Dynamic Stratigraphy: Englewood Cliffs, New Jersey, Prentice-Hall, p. 45-53.

Sloss, L.L., 1962, Stratigraphic models in exploration: Journal of sedimentary petrology, v. 32, n. 3, p. 415-422.

Stanley, D.J., Warne, A.G., and Dunbar, J.B., 1996, Eastern Mississippi delta: late Wisconsin unconformity, overlying transgressive facies, sea level and subsidence: Engineering Geology, v. 45, p. 359-381.

Stow, D.A.V. and M. Johansson, 2000, Deep-water massive sands: nature, origin and hydrocardon implications: Marine and Petroleum Geology, v. 17, p. 145-174.

Straub, K.M., Paola, C., Mohrig, D., Wolinsky, M.A., and George, T., 2009, Compensational stacking of channelized sedimentary deposits: Journal of Sedimentary Research, v. 79.

Strong, N. and Paola, C., 2008, Valleys that never were: Time surfaces versus stratigraphic surfaces: Journal of sedimentary research, v. 78, p. 579-593.

Strong, N., Sheets, B.A., Hickson, T.A., and Paola, C., 2005, A mass-balance framework for quantifying downstream changes in fluvial architecture, *in* Blum, M., Marriott, S., and Leclair, S., eds., Fluvial sedimentology VII, International Association of Sedimentologist, Special Publication 35, p. 243-253.

Swenson, J.B., 2005, Fluviodeltaic response to sea level: Amplitude and timing of shoreline translation and coastal onlap, Journal of Geophysical Research-Earth Surface, v.110, p. F03007, doi:10.1029/2004JF000208.

Syvitski, J. P. M., Kettner, A. J., Overeem, I., Hutton, E. W. H., Hannon, M. T., Brakenridge, G. R., Day, J., Vorosmarty, C., Saito, Y., Giosan, L., and Nicholls, R. J., 2009, Sinking deltas due to human activities: Nature Geoscience, v. 2, p. 681-686, doi: 10.1038/NGEO629.

Tomer, A., Muto, T., and Kim, W., 2011, Autogenic hiatus in fluviodeltaic successions: geometrical modeling and physical experiments: Journal of Sedimentary Research, v. 81, p. 207-217.

Tornqvist, T.E. and Bridge, J. S., 2002, Spatial variation of overbank aggradation rate and its influence on avulsion frequency: Sedimentology, v. 49, p. 891-905.

Van Heijst, M.W.I.M., and Postma, G., 2001, Fluvial response to sea-level changes: a quantitative analogue, experimental approach: Basin Research, v. 13, p. 269-292.

Van Wagoner, J.C., 1995, Sequence stratigraphy and marine to nonmarine facies architecture of foreland basin strata, Book Cliffs, Utah, U.S.A., *in* Van Wagoner, J.C., and Bertram, G.T., eds., Sequence Stratigraphy of Foreland Basin Deposits: Outcrop and Subsurface Examples from the Createaceous of North America, Volume 64, American Association of Petroleum Geologists, Memoirs, p. 137-223.

Wang, Y., Straub, K.M. and Hajek, E.A., 2011, Scale-dependent compensational stacking: An estimate of autogenic time scales in channelized sedimentary deposits: Geology, v. 39, p. 811-814.

Whipple, K.X., Parker, G., Paola, C., and Mohrig, D.C., 1998, Channel dynamics, sediment transport and the slope of alluvial fans: experiment study, Journal of Geology, v. 106, p. 677-693.

Xu, X., and Deng, Q., 1996, Nonlinear characteristics of paleoseismicity in China: Journal of Geophysical Research, v. 101, p. 6209–6231.

Yu, B., Cantelli, A., Marr, J.G., Pirmez, C., O'Byrne, C., and Parker, G., 2006, Experiments on self-channelized subaqueous fans emplaced by turbidity currents and dilute mudflows: Journal of Sedimentary Research, v. 76, p. 889-902.

BIOGRAPHY

After the completion of college entrance examinations in 2004, Yinan Wang was enrolled by China University of Geosciences in Beijing. There he received a bachelor degree in Petroleum Engineering. In December 2009, Yinan attended Department of Earth and Environmental Sciences at Tulane University, where he received a MS degree in Geology. In Tulane's Sediment Dynamics Laboratory, he worked with Professor Kyle Straub to construct experimental deltas and quantitatively analyze the channel stacking architecture. This thesis can be thought of as a summary of his academic gains at Tulane. Yinan plans to return to China and apply for a job in the oil industry or business field.